APPLIED SPECTROSCOPY REVIEWS, 24(3 & 4), 259-312 (1988)

Medical Application of Raman Spectroscopy

YUKIHIRO OZAKI
Division of Biochemistry
The Jikei University School of Medicine
3-25-8, Nishi-shinbashi, Minato-ku, Tokyo 105, Japan

I. INTRODUCTION

In about the last 20 years, Raman spectroscopy has made phenomenal progress owing to technological innovations in lasers, detectors, and computers. Today, application of Raman spectroscopy spreads over large areas of science and technology. Medical science has also become one of the targets of Raman spectroscopy [1]; it has considerable promise as a diagnostic or analytical tool in medicine since it is an excellent nondestructive structural probe for constituents of biological materials [2-6].

Medical application of Raman spectroscopy started as a natural extension of its biological application in the middle 1970s. A couple of landmark works appeared in those days; Thomas et al. [7] and Yu et al. [8] reported Raman studies of intact viruses and eye lenses, respectively, and Larsson and Hellgren [9] proposed blood testing by Raman spectroscopy. Since these pioneering works the medical application of Raman spectroscopy has extended gradually to various areas of medicine. It was the development of multichannel detectors [10, 11] and the advent of the laser Raman microprobe [10, 12-15] that encouraged progress in medical applications. The laser Raman microprobe has played an especially important role in arousing the interest of medical scientists in Raman spectroscopy. Nowadays, one can find examples of Raman spectroscopic application in the fields of physiology [2-6], virology [16, 17], laboratory medicine [9, 18, 19], pathology [20-28], internal medicine [25-27], ophthalmology [29-31], anesthesiology [32], dental surgery [33-37], and urology [28].

In the surge of interest in using Raman spectroscopy in medical science, it is worthwhile surveying the present status of Raman spectroscopy in the medical field and discussing its future prospects. This review treats various aspects of the medical application of Raman spectroscopy. Here, medical application is grouped into four categories. The first category is structural studies on biomedical objects by Raman

spectroscopy and is exemplified by virus research [16, 17]. The second is clinical analysis and testing by Raman spectroscopy; blood testing by "Raman-fluorescence" spectra is one of its topics [9]. The third area is pathological examination by Raman spectroscopy; Raman microprobe detection of inclusions in lung tissue belongs to this category [21]. Clinical diagnosis forms the fourth category and is exemplified by cataract diagnosis [1, 29]. These four categories are dealt with in Sections II, III, IV, and V, respectively. Future prospects for Raman spectroscopy in medical science are discussed in Section VI.

II. STUDIES OF BIOMEDICAL MATERIALS BY RAMAN SPECTROSCOPY

This section is concerned with Raman spectroscopic studies of biomedical materials. These sorts of studies are very important for elucidating the structure and function of their constituents and, at the same time, form the basis for clinical application of Raman spectroscopy. Here, Raman studies of ocular lenses, muscle fibers, viruses, mitochondria, and teeth are discussed. Ordinary biological molecules such as proteins and nucleic acids are not treated in this section because these topics are often reviewed [2-6].

A. Ocular Lenses

An ocular lens refracts the light entering the eye through the pupil and focuses it on the retina [38, 39]. The lens is made up of a number of lens fibers and can be divided into nucleus and cortex. Major constituents of the lens fibers are water and three kinds of structural proteins: α-, β-, and γ-crystallins. The protein content of the lens, about 33% of the total weight, is higher than that of any other organ in the body [38, 39]. Beautiful transparency of the lens is built by the perfect physicochemical arrangement of the lens proteins while its serious disturbance induces lens aging and opacification [38, 39]. The main cause of the disturbance is known to be the formation of protein aggregates [38, 39].

Raman spectroscopy has opened up a new era of lens research [8, 29-31, 40, 41]. This technique has provided a way for investigating the lens proteins under such conditions that the lens maintains its normal physiological state. Raman study of an eye lens has two aspects. One is elucidation of the mechanism of lens aging and opacification at the molecular level. The other is prevision of cataract development by Raman spectroscopy at a precataractous stage. Raman studies of lens

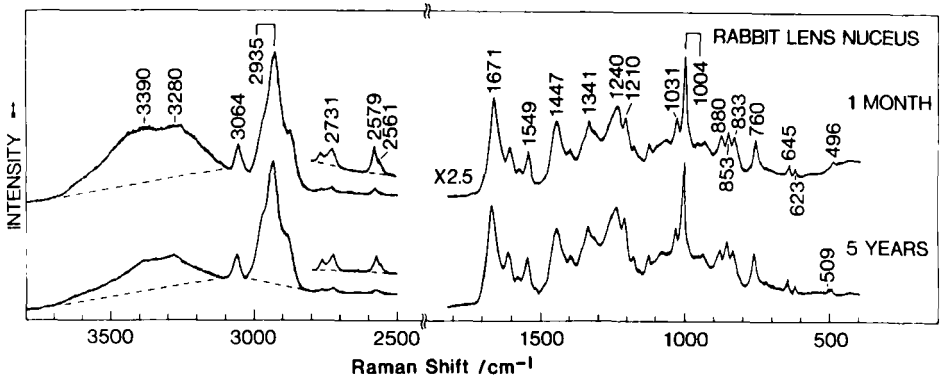

FIG. 1. Whole region of Raman spectra of rabbit lenses (nucleus center, 1 month and 5 years old). Instrumental conditions: excitation wavelength, 488.0 nm; laser power, 120 mW; spectral slit width, 7 cm^{-1}; time constant, 4 s; scan speed, 25 cm^{-1}/min.

aging and cataract development are outlined in this section, and cataract diagnosis by Raman spectroscopy will be discussed in Section V-A.

1. Raman Spectrum of an Ocular Lens

Raman measurement of an intact lens is quite easy unless it is highly turbid. It is also possible to obtain Raman spectrum of a lens directly from a living animal [42]. Figure 1 exhibits the Raman spectra of excised lenses (nucleus center, 1-month-old, and 5-year-old rabbits). The lens spectrum like that in Fig. 1 is, in general, an overlap of the spectra of α-, β-, and γ-crystallins, their derivatives (mainly protein aggregates), and water included in the lens. The entire region of the lens spectrum is rich in important information for exploring lens aging and cataract development [29-31]. For example, the intensity ratio of two Raman bands at 3390 and 2935 cm^{-1} (I_{3390}/I_{2935}), assignable to an OH stretching mode of lens water and CH stretching modes of the lens proteins, respectively, can be used as a practical probe of lens hydration and dehydration. Inter- and intramolecular disulfide bond formation is studied by monitoring intensity decreases of the Raman bands at 2579 and 2561 cm^{-1}, respectively (the 2579 and 2561 cm^{-1} bands are mainly due to SH stretching modes of the "exposed" and "buried" cysteine residues, respectively [43]) (Fig. 1). The frequencies and band shapes of amide I and III bands are key indicators of the secondary structure of the lens proteins. Microenvironmental changes of the tyrosine and tryptophan residues are investigated by the relative

intensity change of a tyrosine doublet near 840 cm^{-1} and the intensity decrease of a tryptophan band at 880 cm^{-1}, respectively.

2. Raman Study of Lens Aging

Lens aging brings about a decline of transparency, lens hardening, and lens pigmentation [38, 39]. The mechanism of lens aging can be investigated in vivo by measuring the Raman spectra of lenses at various stages of aging [29-31]. Recently, Ozaki et al. [43] reported a detailed Raman investigation of the aging process of a SD-strain rat lens. They focused their study on a lens nucleus where only post-synthetic modifications of preexisting proteins occur.

Figure 2(A) displays Raman spectra in the 3800-2800 cm^{-1} region of the rat lens nuclei of 3 and 7 weeks and 13 months old [43]. It is noted that the intensity of the band at 3390 cm^{-1} diminishes clearly with lens aging. This observation indicates that water content in the rat lens

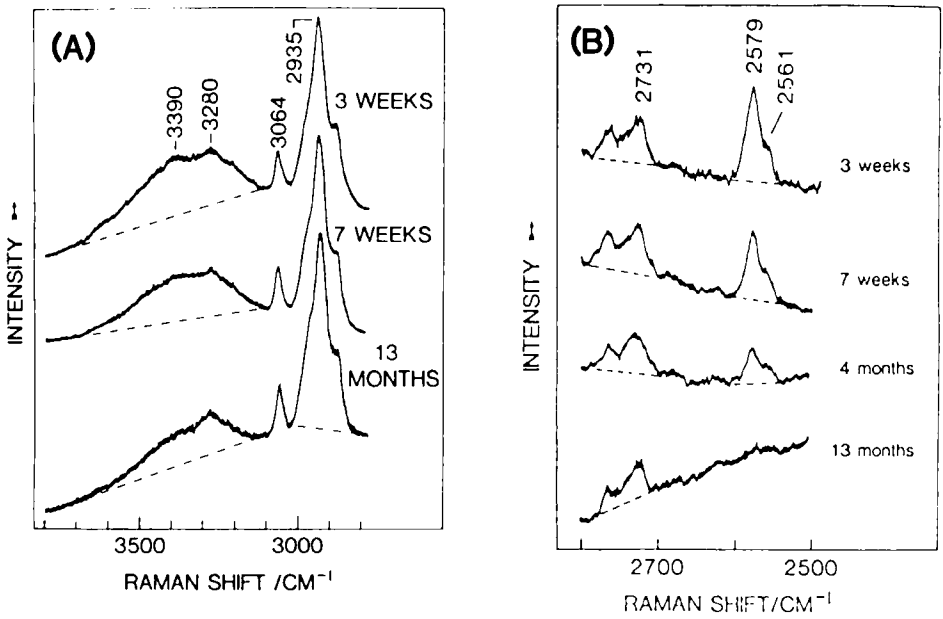

FIG. 2. (A) Age-dependent Raman spectral changes in the 3800-2800 cm^{-1} region of SD-strain rat lens nuclei (3 and 7 weeks and 13 months old). (B) Those in the 2800-2500 cm^{-1} region (3 and 7 weeks and 4 and 13 months old). (Reprinted from Ozaki et al. [43] with permission. Copyright 1987, The American Society for Biochemistry and Molecular Biology.)

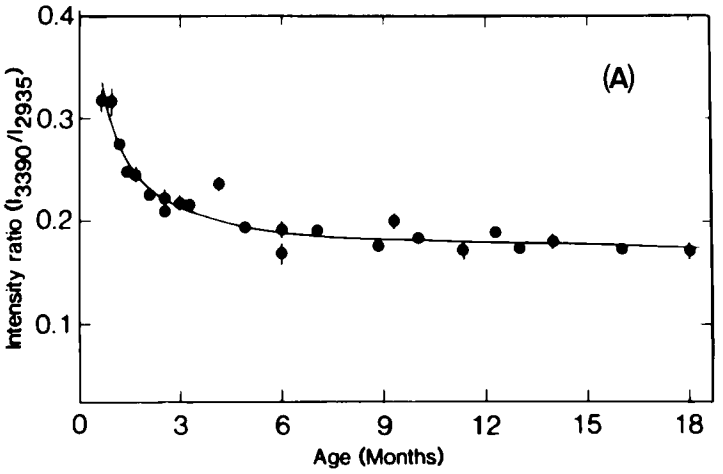

FIG. 3. (A) The intensity ratio of the Raman bands at 3390 cm^{-1} (OH stretching mode of lens water) and 2935 cm^{-1} (CH stretching modes of the lens proteins) versus age for SD-strain rat lens nuclei. (B) That of the bands at 2579 cm^{-1} (SH stretching mode of "exposed" cysteine residues) and 2731 cm^{-1} versus age for SD-strain rat lens nuclei. (C) Correlation between the intensity ratio of (I_{3390}/I_{2935}) and that of (I_{2579}/I_{2731}) for SD-strain rat lens nuclei. (Reprinted from Ozaki et al. [43] with permission. Copyright 1987, The American Society for Biochemistry and Molecular Biology.)

nucleus is reduced considerably in the normal aging process [43]. In Fig. 2(B), age-dependent spectral changes in the 2800-2500 cm^{-1} region of the rat lens nuclei (3 and 7 weeks and 4 and 13 months old) are shown [43]. Particularly striking is that the intensities of the two SH bands decrease dramatically with lens aging. These results, together with the concomitant intensity increase of a band at 509 cm^{-1} due to a S−S stretching mode of protein disulfide bridges, reveal that inter- and intramolecular disulfide bonds are formed in the lens proteins during the course of rat lens aging [43].

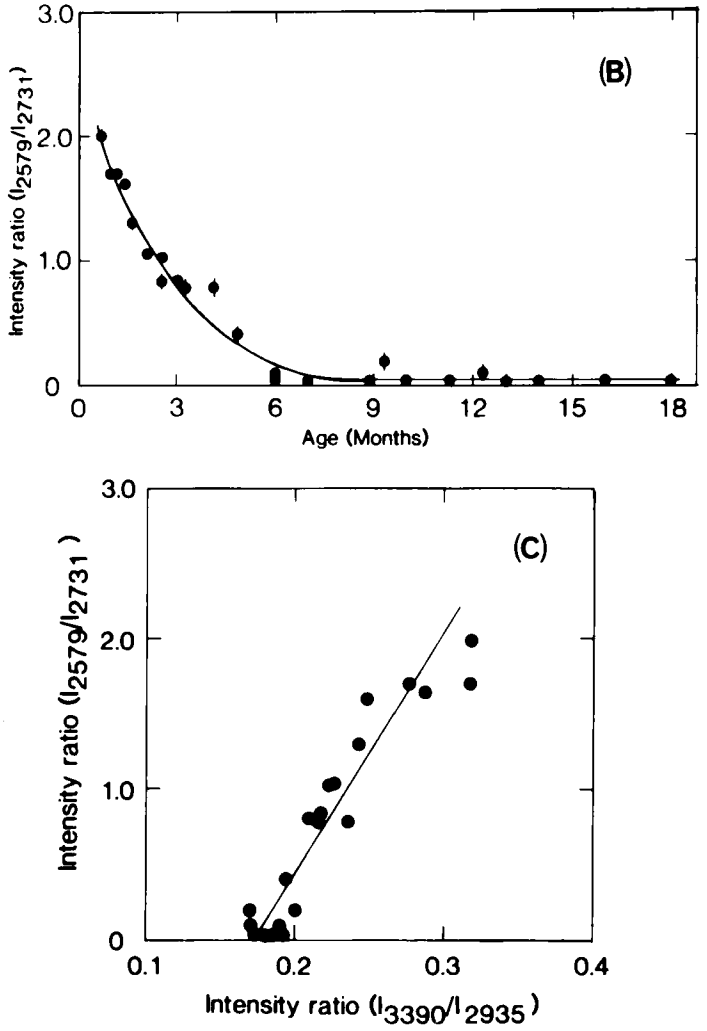

Ozaki et al. [43] found that there is very important correlation between lens dehydration and the formation of intermolecular S–S bonds. Figures 3(A) and 3(B) compare age-dependent profiles of the intensity ratio of the Raman bands at 3390 and 2935 cm^{-1} (I_{3390}/I_{2935}) and that of the intensity ratio of the bands at 2579 and 2731 cm^{-1} (I_{2579}/I_{2731}) for the rat lens nuclei [43]. The two ratios depicted very similar decreasing curves, indicating that lens dehydration and intermolecular disulfide bond formation are related. Figure 3(C) illustrates that there is linear correlation between them. On the basis of the results in

Figures 3(A), 3(B), and 3(C), it is concluded that the intermolecular 2SH → S–S conversion is accelerated by lens dehydration [43]. It seems likely that lens dehydration concentrates the proteins and thus makes the formation of disulfide bonds more feasible. The same conclusion was also reached for ICR-strain mouse [44] and albino rabbit [45] lens nuclei. Two important phenomena, lens dehydration and intermolecular 2SH → S–S conversion, leading to protein aggregation are undoubtedly involved with the decline in transparency and lens hardening.

The secondary structure of the lens proteins in the rat lens nucleus does not undergo a major conformational change with lens aging, but lens aging causes microenvironmental changes in some tyrosine and tryptophan residues [43]. Figure 4(A) compares the Raman spectra in the 950-700 cm^{-1} region between a 3-week-old rat lens nucleus and a 13-month-old one [43]. The intensity ratio of the tyrosine doublet near 840 cm^{-1} (I_{832}/I_{855}), which reflects the nature of hydrogen bonding or

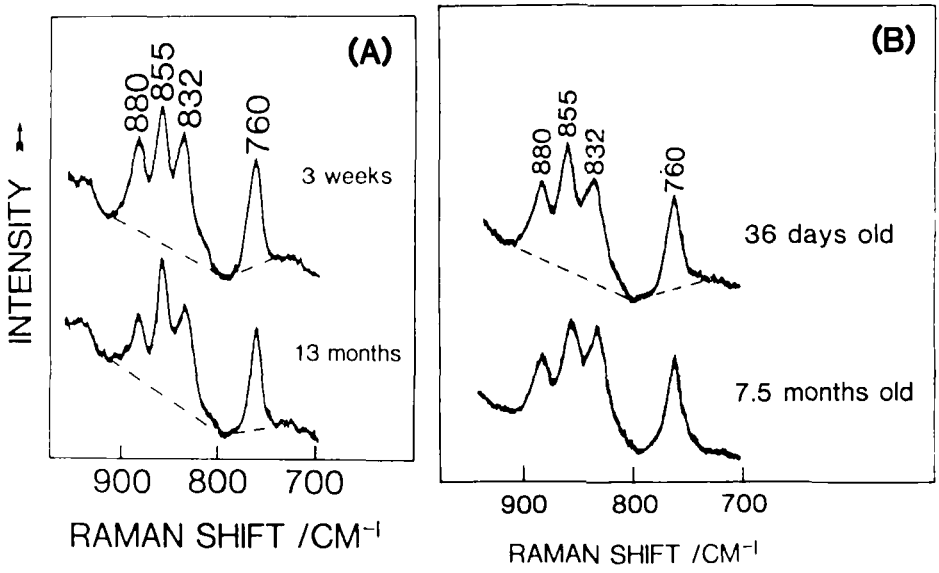

FIG. 4. (A) Raman spectra in the 950-700 cm^{-1} region of 3-week-old and 13-month-old SD-strain rat lens nuclei. (Reprinted from Ozaki et al. [43] with permission. Copyright 1987, The American Society for Biochemistry and Molecular Biology.) (B) Raman spectra in the 950-700 cm^{-1} region of 36-day-old and 7.5-month-old Emory mouse lens nuclei. The former lens was perfectly clear while the latter one was lightly opaque in the nucleus. (Reproduced from Ozaki et al. [51] with permission. Copyright 1987, Society for Applied Spectroscopy.)

the state of ionization of the phenolic hydroxyl group [46], alters from ~0.87 to ~0.81 upon going from the 3-week-old rat lens nucleus to the 13-month-old one. The ratio of two tryptophan bands at 880 and 760 cm^{-1} (I_{880}/I_{760}) also changes from ~0.87 to ~0.66 between the two spectra. It is concluded from these observations that some tyrosine residues undergo a change in their hydrogen bonding environments and some buried tryptophan residues become accessible to water during the course of aging [43]. Of particular importance is that the microenvironmental change of tryptophan residues seems to proceed in parallel with the formation of protein aggregates. This belief comes from the observation that an age-dependent profile of the intensity ratio of the two tryptophan bands (I_{880}/I_{760}) closely resembles that of the relative intensity of the SH band at 2579 cm^{-1} [43]. It is well known that some aromatic amino acid residues of the lens proteins are subjected to chemical modifications and/or photooxidations in the aging process [38, 39]. These phenomena are thought to be implicated in lens pigmentation and opacification. It would therefore be very interesting to investigate whether there is correlation between the observed microenvironmental changes in tyrosine and tryptophan residues and their chemical mofications and photooxidations.

3. Raman Study of Cataract Development

The most remarkable difference from the point of the structure of the lens proteins between lens aging and cataractgenesis is that the molecular weight of protein aggregates found in a cataractous lens is much larger than that of protein aggregates contained in a normally aged lens [38, 39]. Thus far, three pathological (diabetic [47, 48], cac-strain mouse [49, 50], and Emory mouse [51] cataracts) and two experimental (untraviolet-induced [52] and cold [53] cataracts) cataracts have been investigated by Raman spectroscopy.

The Raman studies of cataractous lenses provided three important conclusions. These were concerned with lens hydration [48, 50-52], intermolecular disulfide bridge formation [49, 51], and a microenvironmental change of some tyrosine residues [47, 49, 51, 53]. In contrast to lens aging, the intensity ratio of the two bands at 3390 and 2935 cm^{-1} (I_{3390}/I_{2935}) increases with cataract development except for cold cataract [48, 50-53]. This observation suggests that lens hydration usually occurs in the course of lens opacification. The rate and amount of lens hydration depend on the kind of cataract. The formation of intermolecular disulfide bonds was monitored by Raman spectroscopy for cac-strain mouse [49] and Emory mouse lenses [51] which suffer early-appearing and late-appearing hereditary cataracts, respectively. A comparison of the rate of intermolecular S–S bond formation between a normal

mouse lens and a cac-strain mouse lens or an Emory mouse lens indicates that S−S bond formation in those cataracts is not a predominant factor for initiating the formation of the protein aggregates responsible for lens opacification but for stabilizing them. The mechanism of protein aggregation leading to lens opacification has not been manifested, but it was found by the Raman studies that the aggregation process involves a specific microenvironmental change of tyrosine residues [47, 49, 51, 53]. Figure 4(B) compares Raman spectra in the 950-700 cm^{-1} region of a 36-day-old clear Emory mouse lens nucleus and a 7.5-month-old lightly opaque one [51]. The intensity ratio of the tyrosine doublet clearly changes between them, showing that some tyrosine residues experience a microenvironmental change with cataract development. Interestingly, the direction of the relative intensity change is the reverse of that observed for lens aging [43, 51]. The evidence for microenvironmental change of some tyrosine residues was observed for all the cataracts examined except for ultraviolet-induced cataract [52].

B. Muscle Fibers

Almost 40% of the human body consists of skeletal muscle, so muscle research is very important in clinical medicine as well as in physiology. Muscle fiber is a highly ordered system mainly composed of a protein lattice [54]. The question of whether the contraction of skeletal muscle induces structural changes in contractile proteins such as myosin and actin has been of keen interest. Raman spectroscopy has made a significant contribution to answering this question [55-58].

In order to observe the Raman spectra of intact muscle fibers in both relaxed and contracted states, Pezolet et al. [58] devised a special capillary cell (illustrated in Fig. 5). The use of this cell permits the fibers to be under internal perfusion which insures good control of the concentrations of ATP, Mg^{2+}, and Ca^{2+} [58]. An isolated muscle fiber was gently pulled into the capillary cell in which a small porous tube was inserted. Electrolyte solutions were perfused through the muscle cell by this porous tube. ATP and Mg^{2+} are both essential in the solutions to keep the fibers in the relaxed state, while removal of ATP or Mg^{2+} or addition of Ca^{2+} induces muscle contraction and results in major spectral changes [58].

Figure 6(a) shows the Raman spectrum of a muscle fiber before perfusion [58]. Besides two Raman bands at 1520 and 1156 cm^{-1} assignable to carotenoid chromophores, the observed features come from muscle proteins. Three major features, a relatively sharp amide I band at 1650 cm^{-1}, weak features in the amide III region between 1280

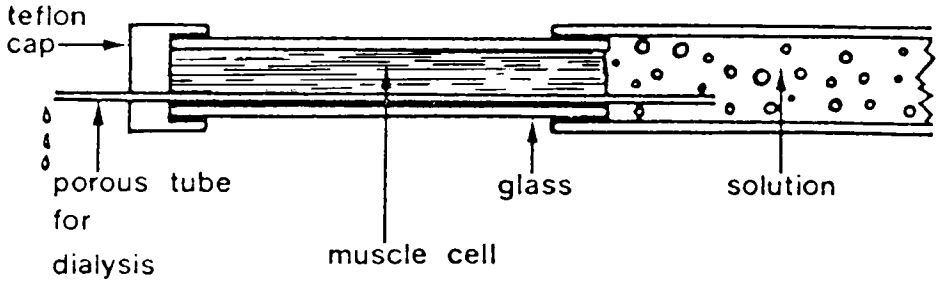

FIG. 5. A specially devised Raman cell for an internally perfused muscle fiber. (Reprinted from Caille et al. [58] with permission. Copyright 1983, Elsevier Science Publishers.)

and 1225 cm^{-1}, and a strong C−C skeletal stretching band at 941 cm^{-1}, indicate that the proteins are mostly in the α-helical conformation [58]. The muscle spectrum is only slightly altered upon perfusion with electrolyte solutions containing both ATP and Mg^{2+}. However, marked spectral changes were observed when muscle contraction was induced by the removal of ATP or Mg^{2+} or the addition of Ca^{2+}. Figure 6(b) illustrates the effect of Ca^{2+} on the Raman spectrum [58]. The spectral changes caused by contraction are clearly recognized in the difference spectrum shown in Fig. 6(c). Particularly notable is that the intensities of the conformational sensitive amide I band at 1650 cm^{-1} and the C−C stretching band at 941 cm^{-1} increase considerably upon contraction. Pezolet et al. [58] interpreted these results as being due to a change of the α-helical content, or of the orientation, of some of the contractile proteins. Another characteristic spectral change in Fig. 6(c) is an intensity decrease of the band at 1412 cm^{-1} due to acidic side chains. This intensity change is thought to arise from strong electrostatic interactions between positively and negatively charged residues of the proteins during contraction [58].

C. Viruses

Viruses are infectious agents which cause various serious diseases to animals and plants [59]. They are rather simple entities and consist essentially of a single nucleic acid molecule (DNA or RNA) encased or encapsulated in a shell (capsid) made up of a large number of identical protein molecules (major coat protein) [59]. The structures of some viruses have been investigated by X-ray crystallography, so that knowledge about viral architecture has been accumulating. However,

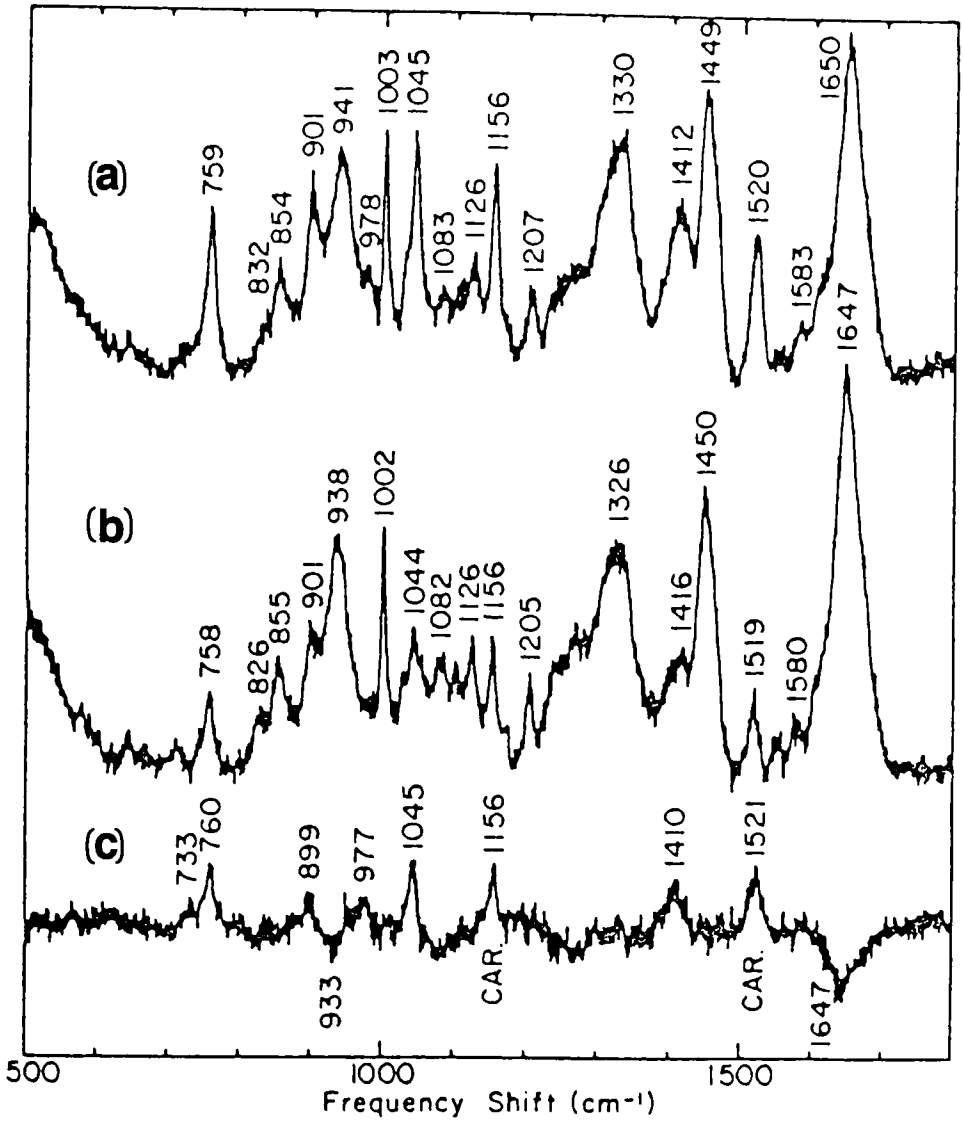

FIG. 6. (a) Raman spectrum of a muscle fiber before perfusion. (b) Raman spectrum of the fiber after 1 h of perfusion with solution containing ATP, Mg^{2+}, and Ca^{2+}. (c) The difference between spectrum (a) and spectrum (b) (a - b) using the 1450 cm^{-1} band as an internal intensity standard; CAR indicates carotenoid bands. (Reprinted from Caille et al. [58] with permission. Copyright 1983, Elsevier Science Publishers.)

relatively few viruses give crystals suitable for X-ray analysis. Moreover, their dynamic structure in aqueous solutions cannot be probed by X-ray crystallography. Accordingly, powerful complementary techniques which offer in situ structural information on a wide variety of viruses and related assemblies are needed.

Raman spectroscopy has played more than a complementary role in structural studies of viruses [16, 17] since Thomas et al. [7] reported the first Raman spectrum of a virus. The Raman spectrum of an intact virus is, in general, an overlap of the spectra of the nucleic acid and protein(s) involved, and therefore yields in situ knowledge about their conformations and interactions [16, 17]. In Raman studies of viruses it is of particular importance to compare the Raman spectra of a mature virus particle, precursor particles or transients in the assembly pathway, and their components so as to reveal changes in intermolecular interactions occurring in virus morphogenesis. Further, Raman measurements under different conditions are very useful for investigating conformational changes and flexibilities of nucleic acid and protein components since their conformations and interactions are very susceptible to environmental factors such as ambient pH, ionic strength, and/or temperature.

Although the principles established for obtaining and interpreting the Raman spectra of nucleic acids and proteins are basically applied to the Raman studies of viruses, they often require special tactics because of the complexity of virus structures and their potential vulnerability to laser irradiation. Regarding this, the reader is referred to recent reviews by Thomas [16, 17].

Viruses can be classified in a couple of ways [59]. Based on the type of host, they are divided into animal, plant, and bacterial viruses (bacteriophages). A number of plant viruses and bacteriophages have been subjected to Raman measurements [16, 17]. In this review the Raman study of filamentous bacteriophages by Thomas et al. [60-63] is discussed as an example.

Figure 7 presents the Raman spectra of Class I (fd, If1, and IKe) and Class II (Pf1, Xf, and Pf3) filamentous bacteriophases [61]. The difference between Class I and Class II phages is based upon the filament symmetry; Class I and Class II structures show $C_5S_{2.0}$ and $C_1S_{5.4}$ symmetry, respectively. The viral genome of the filamentous viruses is single stranded DNA. Because of the low nucleic acid content (~6-14%), the spectra in Fig. 7 are dominated by Raman bands arising from the coat protein [61]. An intense amide I band is observed near 1649 cm^{-1} for all the viruses, suggesting that their coat proteins are α-helical. Raman features in the amide III band region indicate that the protein subunits of Xf and Pf3 include irregular and β-stranded structure,

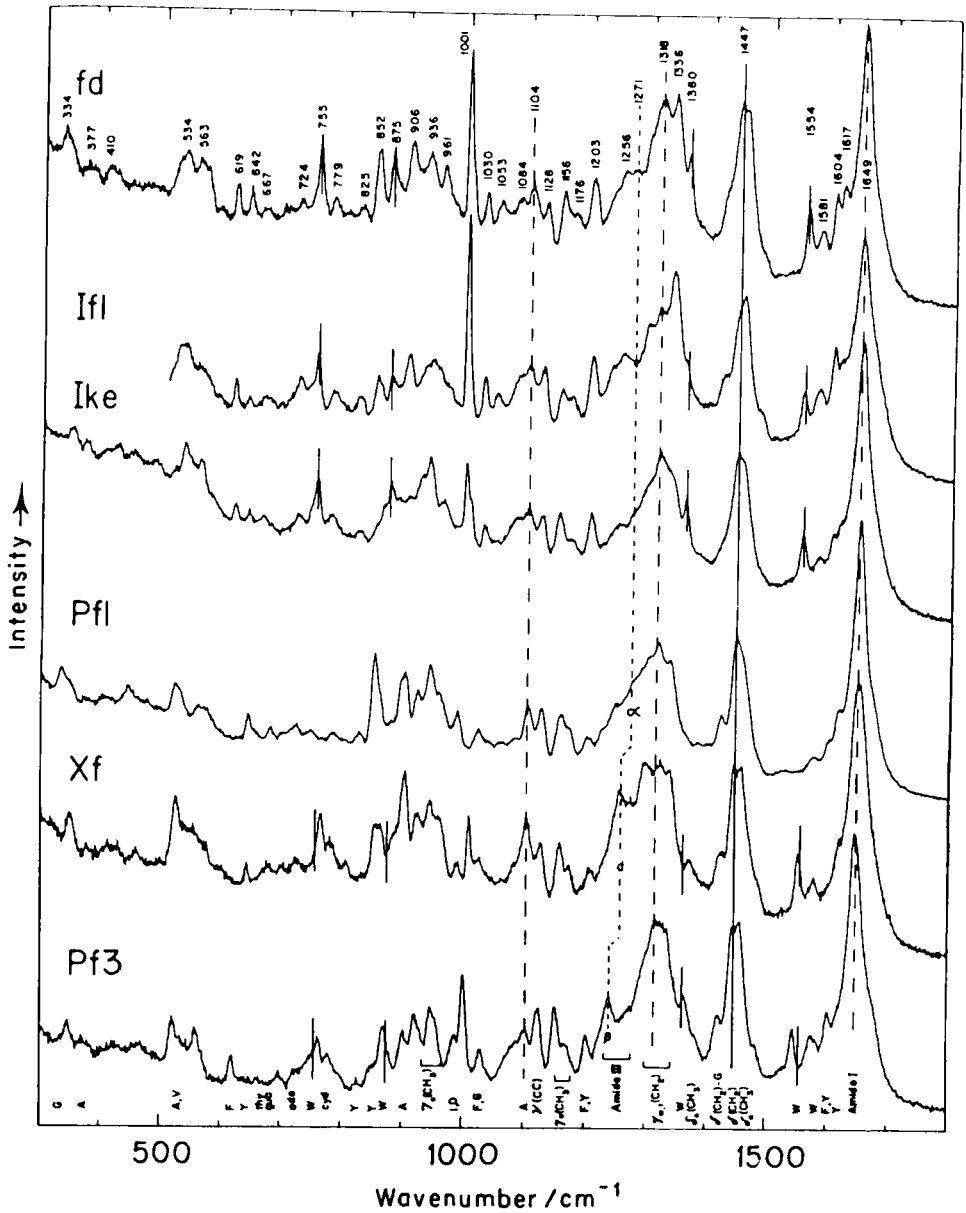

FIG. 7. Raman spectra in the 1800-300 cm^{-1} region of six filamentous viruses: fd, If1, IKe, Pf1, Xf, and Pf3. (Reprinted from Thomas et al. [61] with permission. Copyright 1983, Academic Press (London).)

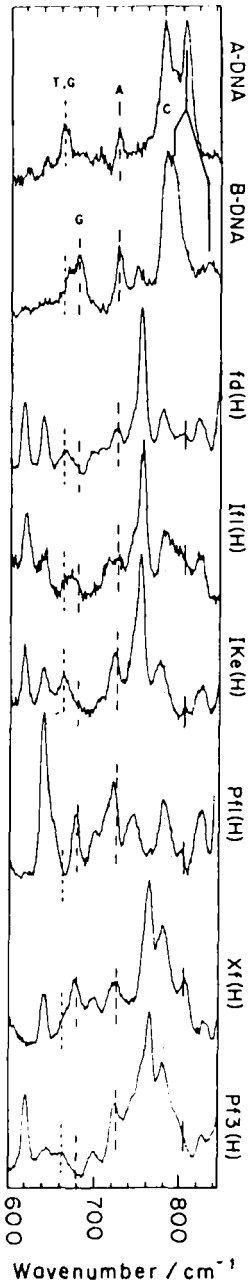

FIG. 8. Raman spectra in the 840-600 cm^{-1} region of six filamentous viruses at high salt concentration and of A- and B-DNA. The broken vertical lines indicate the positions of nucleoside markers while the unbroken ones (at 830 and 810 cm^{-1}) denote those of expected bands of A- and B-DNA backbones. (Thomas et al. [61] with permission. Copyright 1983, Academic Press (London).)

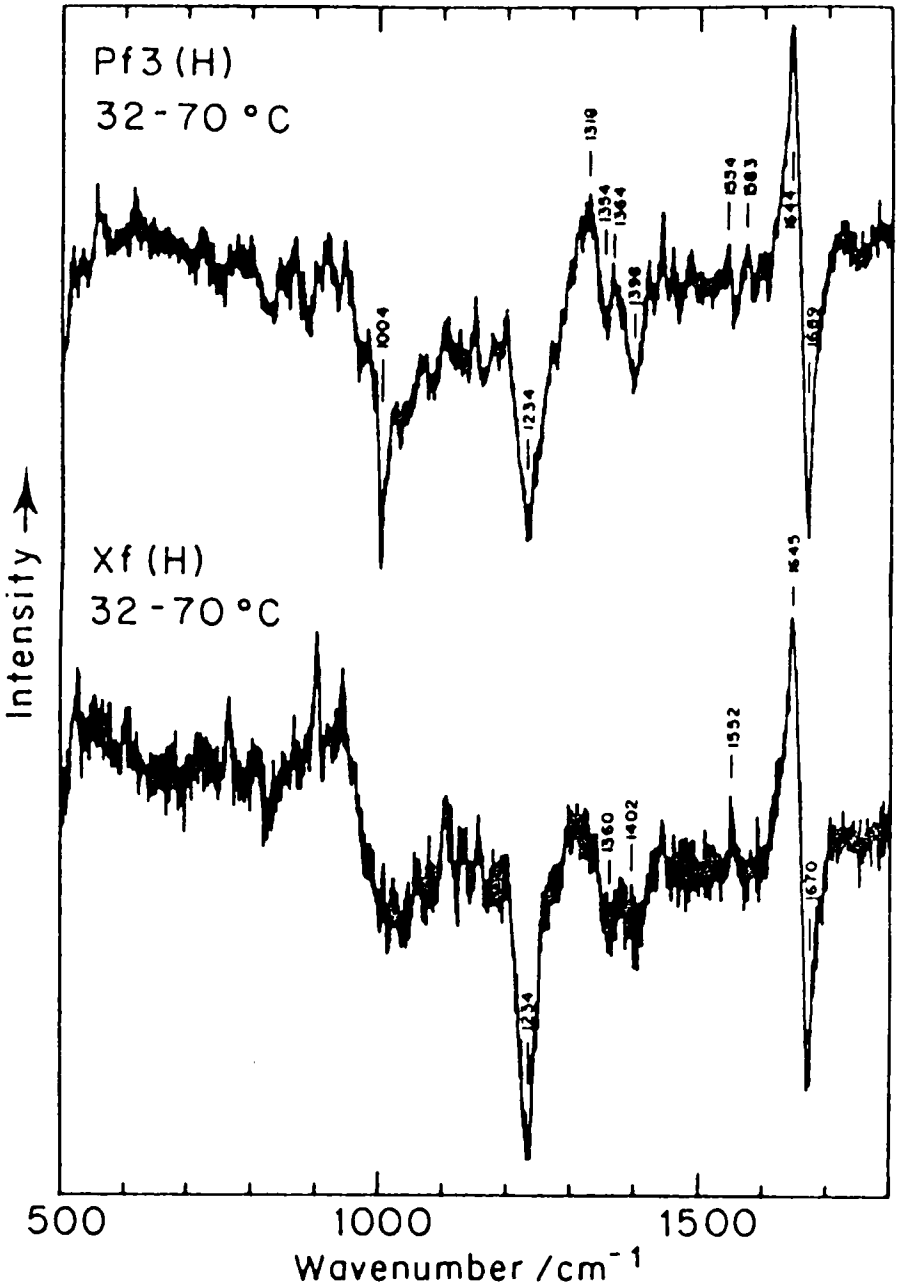

FIG. 9. Raman difference spectra showing α-to-β secondary structure transition between 32 and 70 °C in Pf3 and Xf. (Reprinted from Thomas et al. [61] with permission. Copyright 1983, Academic Press (London).)

respectively. By use of Fourier deconvolution of the amide I band envelope, Thomas [63] estimated the α-helix content of the subunits of fd, If1, IKe, Pf1, Xf, and Pf3 to be 92, 90, 93, 100, 71, and 82%, respectively. The subunits of Class II phages undergo reversible α-to-β secondary structure transitions. The Raman difference spectra shown in Fig. 8 illustrate the large-scale structure transitions observed for Xf and Pf3 subunits between 32 and 70°C [61]; the positive peak near 1645 cm^{-1} is assignable to α-helix while the negative peaks near 1670 and 1234 cm^{-1} are attributed to β-strand structure.

DNA nucleoside conformations were investigated by conformation-sensitive bands appearing in the 850-600 cm^{-1} region [61]. Enlargements of that region are shown in Fig. 9 where the spectra of A- and B-DNA are also included for reference [61]. The broken vertical lines denote the positions of characteristic bands of nucleosides while unbroken ones indicate the positions of the expected bands of A- and B-DNA backbones. These assignments were made by comparison of the Raman spectra of the six viruses with those of their isolated proteins [61]. Particularly notable in the spectra of Fig. 9 is the general absence of characteristic bands for A- and B-DNA backbones. This observation suggests unusual DNA backbone structures for the six viruses [61]. The frequencies and band shapes of the nucleoside markers suggest that the nucleoside conformations of Class I phages are similar to each other, but different from those of Class II phages. Among Class II structures, the nucleoside conformations of Pf1 and Xf are similar to one another, but different from that of Pf3 [61].

The Raman data suggest that DNA bases interact with protein aromatic groups of the C-terminal domain in all six viruses [61].

Microenvironments of tyrosine and tryptophan residues were investigated by the intensity ratio of a tyrosine doublet near 840 cm^{-1} and the relative intensities of bands near 1360 and 880 cm^{-1}, respectively [61]. The phenolic OH groups of all tyrosine residues of fd, If1, Pf1, and Xf are acceptors of strong hydrogen bonds from highly positive donors, while that of the tyrosine residue of IKe is hydrogen bonded to both donor and acceptor groups. Tryptophan residues of fd, If1, and IKe are buried in the proteins. In contrast, those of Xf and Pf3 are in anomalous environments which could arise from specific contacts with charged or polar groups of the DNA.

Approaches similar to those employed in virus research have been successfully applied to Raman studies of related nucleoproteins such as ribosomes, chromatin, and nucleosomes, and gene regulatory complexes [16, 17].

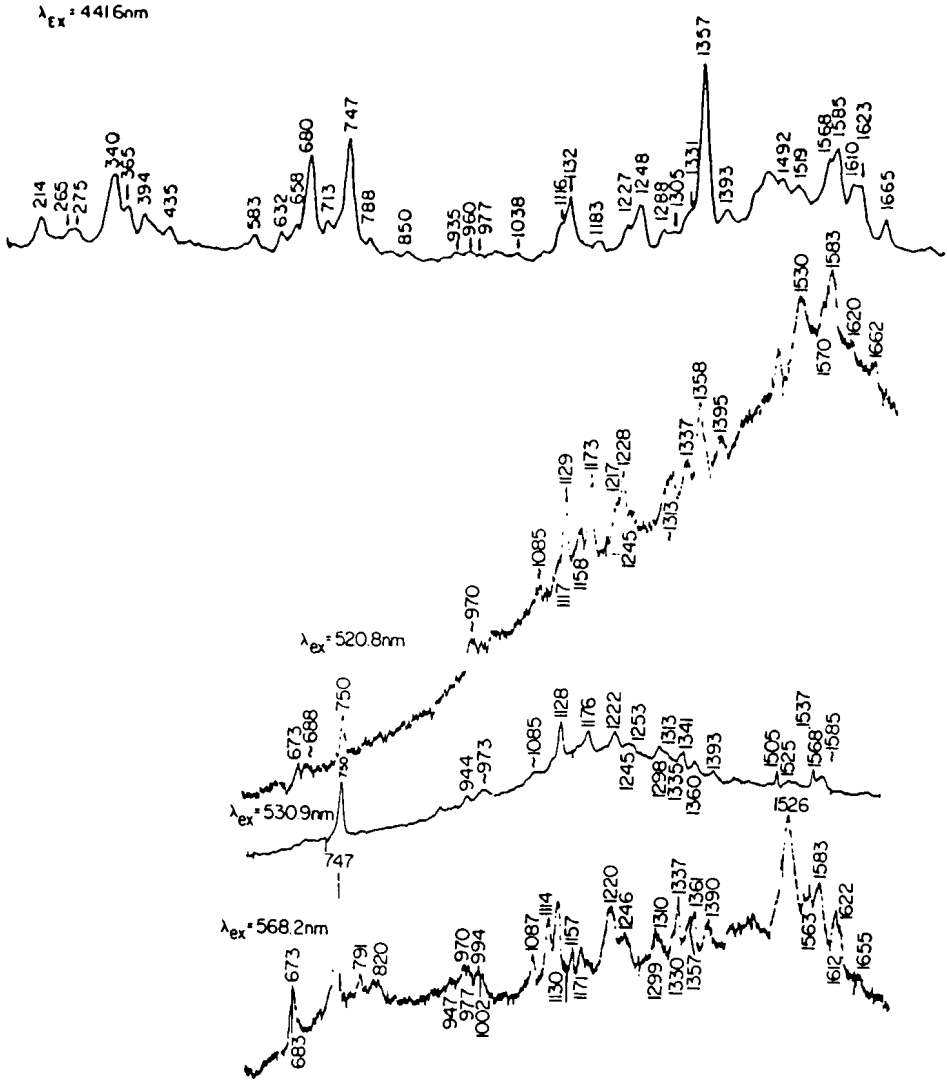

FIG. 10. Resonance Raman spectra of whole mitochondria excited at 568.2, 530.9, 520.8, and 441.6 nm. Samples were reduced with minimal amounts of dithionite. (Reproduced from Adar and Erecinska [64] with permission. Copyright 1978, American Chemical Society.)

D. Mitochondria

If it were possible to measure the Raman spectra of nucleus and organelle at one's will, Raman spectroscopy would become a powerful investigative tool not only in cell biology but also in cell diagnosis. Adar and Erecinska [64] succeeded in measuring resonance Raman (RR) spectra of whole mitochondria. Their work was not performed in situ, but it demonstrated the potential of RR spectroscopy for studying subcellular materials. Figure 10 shows the RR spectra of whole mitochondria excited at 441.6, 520.8, 530.9, and 568.2 nm [64]. The sample, extracted from the muscle cell of pigeon breast, was suspended in 100 mM phosphate buffer, pH 7.4, and reduced with dithionite. Final sample concentration as estimated by the cytochrome a content was of the order of 20-30 mM [64]. The overall appearance of the RR spectra changes with the excitation wavelength. In order to identify the contributions of the constituents of mitochondria to the RR spectra, they compared them with the spectra of cytochrome oxidase, B and C type cytochromes, and cytochrome b-c_1 complex [64]. The comparison indicated that the 568.2- and 441.6-nm excited RR spectra of whole mitochondria consist almost completely of those of cytochrome b and cytochrome oxidase, respectively, while the 530.9- and 520.8-nm excited ones are very close to those of the cytochrome b-c_1 complex. It is very unlikely that mitochondrial components other than cytochromes make a detectable contribution to the RR spectra. The strong dependence of the spectral pattern on the excitation wavelength is caused by the RR effect which reflects the relative position between the excitation wavelength and absorption maxima of the α-, β-, and γ-bands of the cytochromes. The use of the RR effect allowed them to investigate mitochondrial cytochromes selectively.

Adar and Erecinska [64] found significant differences between the RR spectra of purified cytochromes and the same components in whole mitochondria. The following two differences are particularly noteworthy. (1) Marker bands for B-type cytochromes near 1565, 1535, and 1305 cm^{-1} show a downward shift by 5-6 cm^{-1} in the RR spectra of whole mitochondria. (2) Another marker band for B-type cytochromes near 1340 cm^{-1} splits in the mitochondrial system. These spectral changes in mitochondrial complexes are thought to be due to heme-heme interactions and/or to alterations in the hemes' environments [64]. Although the cause of the changes has not yet been clarified, these spectral differences indicate the potential of RR spectroscopy as a nondestructive structural probe for mitochondrial constituents.

E. Teeth

Human tooth enamel and dentin have long been the subjects of extensive studies for the prevention of tooth decay as well as of biological interest [65]. Several research groups have employed Raman spectroscopy for investigations of enamel and dentin since the first report of the Raman spectra of tooth by O'Shea et al. [33]. Yamada et al. [34] carried out paleobiophysical studies of tooth tissues by the use of Raman spectroscopy. Nishigori et al. [35] investigated the difference between human and shark teeth by the same technique. Moreover, Suzuki et al. [37] performed a Raman study of the adhesive inter-

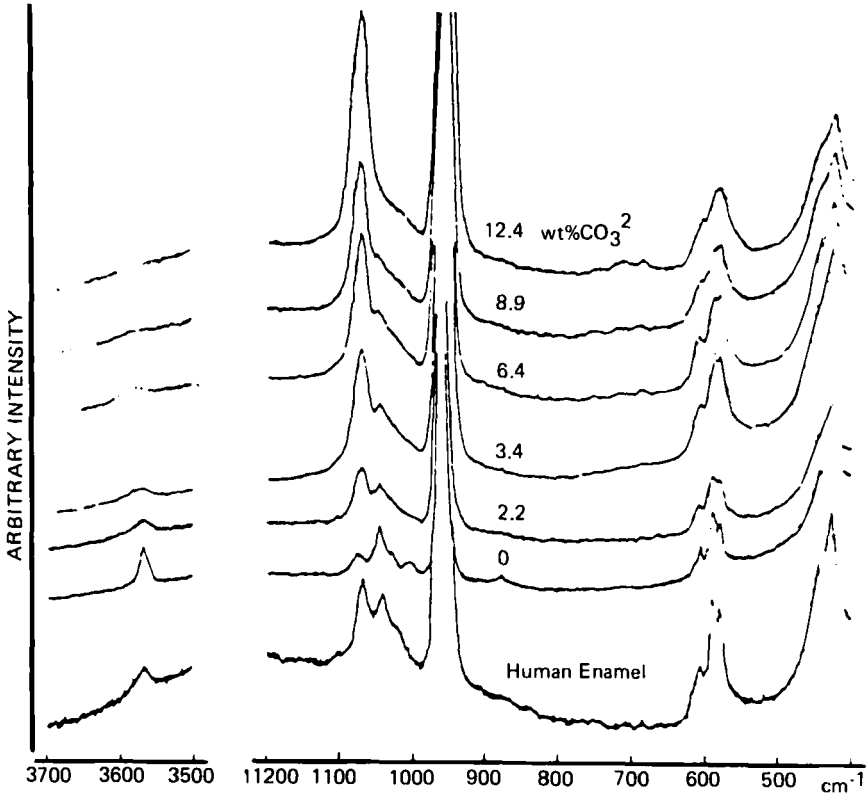

FIG. 11. The 514.5-nm excited Raman spectra of human tooth enamel and synthetic apatites containing from zero to 12.4% (w/w) carbonate ions. (Reprinted from Nishino et al. [36] with permission. Copyright 1981, The American Association for Dental Research.)

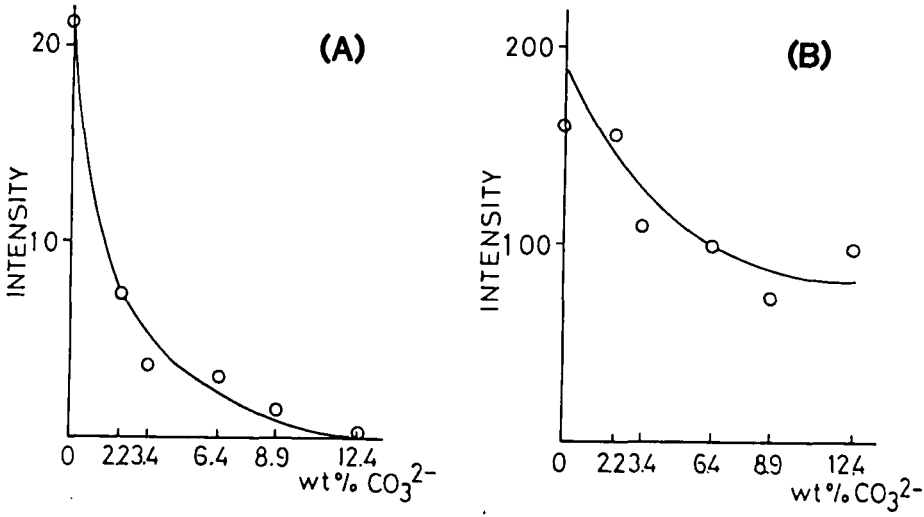

FIG. 12. (A) Correlation between the relative intensity of the OH stretching band and the CO_3^{2-} content. (B) Correlation between the relative intensity of the PO_4^{3-} γ_1 band and the CO_3^{2-} content. (Reprinted from Nishino et al. [36] with permission. Copyright 1981, The American Association for Dental Research.)

face between dentin and dental adhesives. In this section a comparative Raman study of human enamel and synthetic carbonate-containing apatites by Nishino et al. [36] is discussed in some detail.

Carbonate-containing apatites are a major ingredient of human tooth enamel [65]. Carbonate ions content has been estimated to be 1.95-3.66% in weight, and their presence is implicated to the caries susceptibility of the enamel [65]. Investigation of the nature and location of the carbonate ions is therefore very important. Nishino et al. [36] compared the Raman spectrum of the enamel with those of synthetic apatites containing from zero to 12.4% (w/w) carbonate ions. Figure 11 exhibits their Raman spectra in the 3700-3500 and 1200-400 cm^{-1} regions. Vibrational assignments of Raman bands of the enamel were made first by O'Shea et al. [33]; Raman bands at 3567, 1066, 1040, and 956 cm^{-1} are assigned to an OH stretching, CO_3^{2-} γ_1, PO_4^{3-} γ_3, and PO_4^{3-} γ_1 modes of the carbonate-containing apatites, respectively (the 1066 cm^{-1} band includes a small contribution from the PO_4^{3-} γ_3 mode), and a group of bands near 700, 590, and 440 cm^{-1} are attributed to their CO_3^{2-} γ_4, PO_4^{3-} γ_4, and PO_4^{3-} γ_2 modes, respectively. The Raman spectra of the synthetic carbonate-containing apatite series bear

a general resemblance to that of the enamel and exhibit progressive changes in intensity with an increase in the CO_3^{2-} content. The intensities of the CO_3^{2-} γ_1 and γ_4 modes increase conspicuously, while those of the OH stretching mode and the PO_4^{3-} γ_3 and γ_1 modes decrease considerably as a function of the CO_3^{2-} content.

A comparison of the Raman spectrum of human tooth enamel with those of synthetic specimens shows that the enamel spectrum most closely resembles the spectrum of the synthetic apatite which contains 2.2 or 3.4% (w/w) CO_3^{2-}. This finding is consistent with the chemical analytical data previously reported [66]. Furthermore, Nishino et al. [36] obtained information about the substitution sites of CO_3^{2-} in the apatite lattice from their Raman study. Figures 12(A) and 12(B) illustrate the correlation between the intensity of the OH stretching mode (A) and that of the PO_4^{3-} γ_1 mode (B) with the CO_3^{2-} content [36]. The results shown in Fig. 12, together with the observation of the concomitant intensity increases of the CO_3^{2-} γ_1 and γ_4 modes, led them to conclude that the CO_3^{2-} incorporated in the apatite lattice substitutes not only for PO_4^{3-} but also for OH^- [36].

The CO_3^{2-} content and its location in the apatite had been studied previously by infrared spectroscopy and X-ray diffraction, and thus the conclusions reached in the Raman study are not novel. However, it should be noted that Raman spectroscopy is capable of examining intact teeth directly. Further investigations of the Raman spectra of human teeth may reveal correlation between the intensities of Raman bands due to the OH, CO_3^{2-}, and PO_4^{3-} groups and the CO_3^{2-} content or its location in the tooth enamel, and future in situ diagnosis of teeth by Raman spectroscopy may be possible.

III. CLINICAL ANALYSIS AND TESTING BY RAMAN SPECTROSCOPY

Clinical analysis and testing (e.g., blood tests) are often grounds for the diagnosis of a disease. Many spectroscopic methods are employed in laboratory medicine because they are usually superior in sensitivity, reproducibility, rapidity, and economical efficiency, and they do not require a large amount of sample. Raman spectroscopy may also become a unique tool for clinical analysis and testing. This section takes up four examples of clinical analysis and testing by Raman spectroscopy.

A. Blood Test by "Raman-Fluorescence" Spectra

Blood tests are important for diagnosing a disease and monitoring the condition of a patient. However, drawing a large amount of blood often burdens a patient. A blood test proposed by Larsson and Hellgren [9] requires only 0.1 mL of blood and gives reliable results on the condition of a patient in a few minutes. They compared the Raman spectra of blood plasma from patients suffering from various diseases such as hepatitis, leukemia, and carcinoma with those of healthy controls [9]. Only 0.1 mL of blood plasma was employed for each Raman measurement. The Raman spectra of the blood plasma of patients were distinguishable at a glance from those of healthy controls and depended more or less upon the kinds and conditions of diseases.

Figure 13(A) illustrates the 514.5-nm excited Raman spectrum of blood plasma from a 23-year-old healthy woman [9]. The broad feature centered near 3350 cm^{-1} consists of several bands assignable to OH and NH stretching modes, while the shoulder near 2900 cm^{-1} may be due to CH stretching modes. The intense bands at 1520 and 1160 cm^{-1} are assigned to C=C and C−C stretching modes, respectively, of a carotenoid. The spectra of all normal cases exhibit characteristics similar to those of the spectrum in Fig. 13(A), irrespective of sex and age.

The Raman spectrum of blood plasma from a patient (20-year-old woman) with homologous serum hepatitis is shown in Fig. 13(B). Marked spectral changes are seen between Spectra (A) and (B) in Fig. 13. In the latter spectrum, background fluorescence is conspicuously strong and two intense bands due to the carotenoid are only barely observed. It is indeed a "Raman-fluorescence" spectrum. Figure 13(B') exhibits the spectrum taken 20 days later when the patient had clinically recovered [9]. The dramatic spectral changes from Fig. 13(B) to Fig. 13(B') illustrate how the curve is normalized when the patient becomes healthy. Figures 13(C) and 13(D) display Raman spectra of blood plasma from a 62-year-old woman with infiltrating mammary carcinoma and from a 64-year-old woman with pseudomucinous papillary cystadenocarcinoma, respectively [9]. The spectra of Figs. 13(B), 13(C), and 13(D) look similar, but they are considerably different in detail [9]. For example, the fluorescence peaks of Figs. 13(B), 13(C), and 13(D) are located near 3400, 3500, and 3600 cm^{-1}, respectively. Moreover, the blood plasma of patients with pathologically high lipid content always gives pronounced maximum near 2900 cm^{-1} due to the CH stretching modes.

On the basis of the above results, along with those of other cases, Larsson and Hellgren [9] came to the conclusion that the Raman measurement of blood plasma is very useful for indicating the presence of a disease and for monitoring the condition of a patient. They also

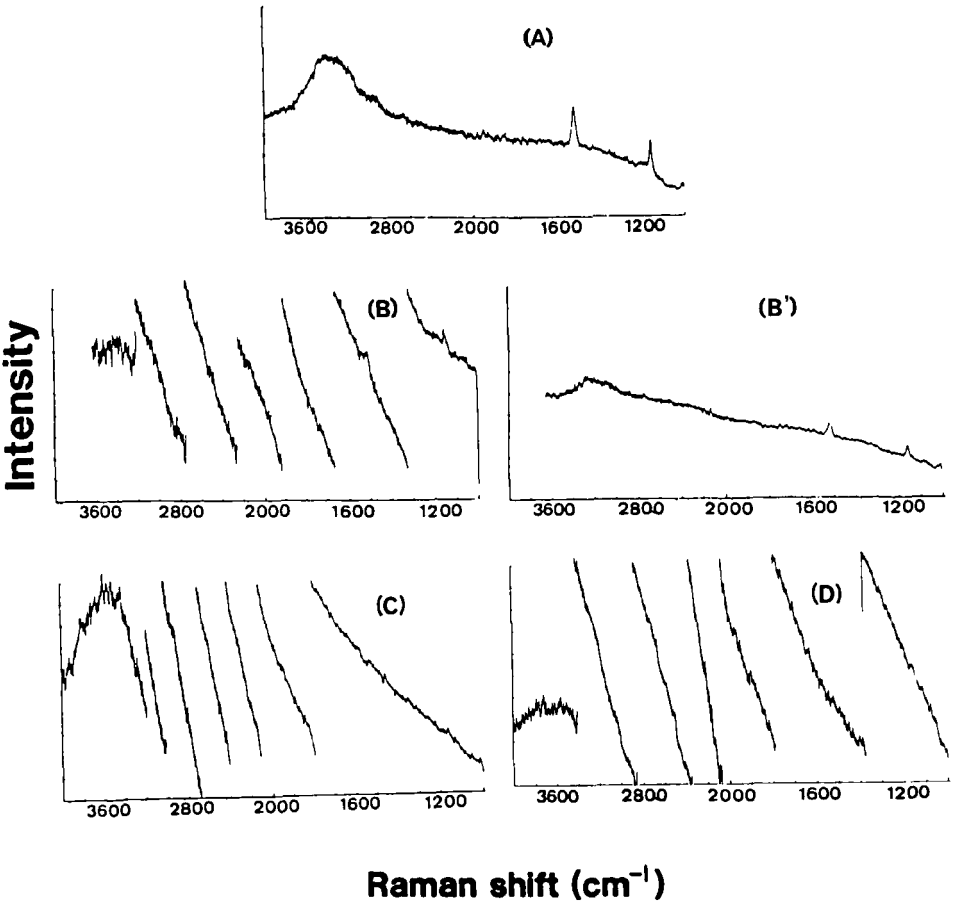

FIG. 13. (A) Raman spectrum of blood plasma from a 23-year-old healthy woman. (B), (B') Raman spectra of blood plasma from a 20-year-old woman with homologous serum hepatitis. The spectrum (B) was recorded during the icteric period while that of (B') was taken 20 days later when the patient was clinically recovered. (C) Raman spectrum from a 62-year-old woman with infiltrating mammary carcinoma. (D) Raman spectrum from a 64-year-old woman with pseudomucinous papillary cystadeno carcinoma, respectively. (Reproduced from Larsson and Hellgren [9] with permission. Copyright 1974, Birkhauser Verlag.)

TABLE 1

Comparison between "Raman-Fluorescence" Method and Erythrocyte Sedimentation Rate (ESR)

	Healthy controls	Diseased patients
ESR:		
Normal	13	21
Pathological	0	32
"Raman-fluorescence":		
Normal	13	0
Pathological	0	53

compared their "Raman-fluorescence" method with the measurement of the erythrocyte sedimentation rate (ESR). Table 1 shows the result of the comparison; the Raman-fluorescence method gave a pathological spectrum for all the patients examined while the ESR test provided normal results for 21 patients [9]. This comparison suggests that the Raman-fluorescence spectrum is more sensitive than ESR for various pathological disturbances affecting the plasma. It seems worthwhile to put the above blood test to practical use because of its high sensitivity, simplicity, and low cost.

B. Determination of Thiol Concentrations in Hemolysate by Resonance Raman Spectrometry

Determination of thiol concentrations in hemolysate is of considerable importance in clinical medicine because thiols perform a vital role in various intracellular processes [67]. In measurement of biological thiol content, however, the problem of artificial oxidation of thiol to disulfide is often encountered. To overcome this problem the exchange reaction of SH groups with N-ethylmaleimide or 5,5'-dithiobis(2-nitrobenzoic acid) (Ellman's reagent) (ESSE) is generally employed [67]:

$$\mathrm{ESSE} + \mathrm{RSH} \rightleftharpoons \mathrm{ESSR} + \mathrm{ESH} \qquad (1)$$

Banford et al. [19] reported a simple and sensitive method for determining the thiol concentration in hemolysate by means of the RR

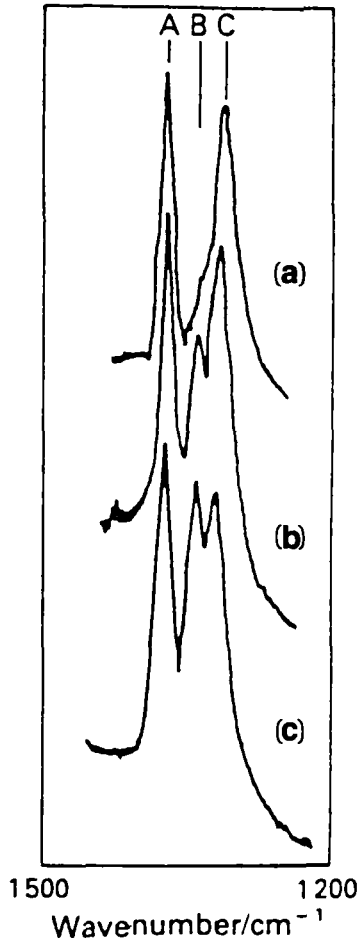

FIG. 14. RR spectra of the reaction products of hemolysate with Ellman's reagent. A 5-fold, a 20-fold, and a 100-fold excess of Ellman's reagent were used in Spectra (a), (b), and (c), respectively. (Reprinted from Banford et al. [19] with permission. Copyright 1982, The Royal Society of Chemistry.)

spectrum of the reaction product (ESH) of the lysate with Ellman's reagent. ESH (hereafter, E denotes 2-nitrobenzoic acid) is ionized to ES^- at the neutral pH employed for the determination. Figure 14 displays the 457.9-nm excited RR of the reaction mixture of the hemolysate with Ellman's reagent [19]. The 457.9-nm excitation gives a high-quality RR

spectrum since this wavelength is close to the absorption maximum (412 nm) of the ES^- group. Bands A (1373 cm^{-1}), B (1348 cm^{-1}), and C (1325 cm^{-1}) in Fig. 14 are due to hemoglobin, ESSE, and ES^-, respectively. The difference among Spectra (a), (b), and (c) comes from the difference in the amount of ESSE added; in Spectrum (a) a 5-fold excess, in Spectrum (b) a 20-fold excess, and in Spectrum (c) a 100-fold excess of ESSE were used. Banford et al. [19] employed the hemoglobin peak as an internal calibrant to estimate the band area of the thiol peak. To determine the thiol concentration per hemoglobin molecule, standard additions of glutathione were made to the hemolysate. Hemoglobin concentrations are routinely obtained in blood tests, and therefore the absolute determination of thiol concentrations is easily carried out. The mean value of the lysate thiol concentrations determined by their method was 1920 ± 88 μm for 6 male volunteers [19]. The corresponding value for 7 patients with rheumatoid arthritis was appreciably higher (3240 ± 774 μm), suggesting that their measurements may be very useful in the study of disease processes [19].

C. Catecholamine and Drug Analysis by Resonance Raman and Surface-Enhanced Raman Scattering Spectrometries

Microanalysis of biological molecules and drugs is very important in medical science. In the last two decades a variety of modern analytical methods has been introduced for microanalysis in the medical field. Nowadays, trace determinations at subnanogram levels can be carried out for various kinds of biological samples.

1. Catecholamine and Drug Analysis by RR Spectrometry

It had been almost unthinkable to employ Raman spectroscopy for the trace analysis of biological molecules because of its low sensitivity before RR spectrometry came into general use. The RR technique is a sensitive and selective analytical tool for nonfluorescent molecules of biomedical interest. Attempts at using this technique for the trace analysis of biological molecules began in the mid-1970s. Morris et al. [68-70] used RR spectrometry for the determination of catecholamines. In those days catecholamines were analyzed by the fluorometric trihydroxyindole procedure in which they are converted into fluorescent trihydroxyindole via aminochromes. Morris et al. [68-70] noticed that the aminochromes have suitable chromophores (λ_{max} = 480-500 nm) for RR spectrometry, and they measured the RR spectra of aminochromes of several catecholamines such as adrenaline, noradrenaline, and dopamine. The spectra obtained were characteristic of each catecholamine. The most useful bands for catecholamine determination are a pair of

bands observed in the 1480-1415 cm^{-1} region [68-70]. These bands contain a large contribution from the $C=N^+$ stretching mode and are thus sensitive to substituents in the five-membered ring of aminochromes. According to them [68-70], the detection limits for adrenaline, noradrenaline, isoproterenol, and dopamine by aminochrome RR spectrometry are about 2×10^{-6} M. These limits are higher than those for fluorometry. However, the usual catecholamine analysis involves a preconcentration procedure, so the catecholamine concentrations may be brought within the detection limits of RR spectrometry. The clear advantage of the RR method is the simultaneous determination of several catecholamines in a single sample [68-70].

Sato et al. [71] applied the same technique to the determination of small amounts of sulfonamide drugs. The sulfonamide drugs, which have a general structure of the type $H_2N-C_6H_4-SO_2-NH-R$, where R is H, $C(NH)NH_2$, or a heterocyclic group, are of considerable therapeutic value. Aqueous solutions of these drugs give characteristic Raman spectra, as shown in Fig. 15(A), but they do not exhibit an RR effect under visible excitations [71]. They were therefore converted by diazotization to colored derivatives from which RR spectra can be obtained. Figure 15(B) displays the 488.0-nm excited RR spectra of the azo derivatives ($R''-N=N-C_6H_4-SO_2NH-R$; R'' represents the N-(1-naphthyl)ethylenediamine substituent) of several sulfonamides (2×10^{-5} M aqueous solutions) [71]. These solutions provide high quality Raman spectra with the aid of the RR effect. The detection limits, about 2×10^{-8} M, are approximately an order of magnitude higher than that of standard colorimetry. However, the method is not suitable for the identification of individual sulfonamides because Spectra (a), (b), (c), and (d) are almost identical. However, the method may be used to indicate the presence of sulfonamides. Sato et al. [71] found that characteristic RR spectral patterns can be obtained from the colored derivatives of sulfonamides produced by hydrolysis.

2. Drug Analysis by Surface-Enhanced Raman Scattering Spectrometry

The use of the RR effect dramatically raised the potential of Raman spectroscopy as an analytical tool. However, the detection limits for RR spectrometry are, in general, high compared with those given by such other techniques as fluorometry and mass spectrometry. Recent findings of enhanced Raman scattering from molecules at or near metallic surfaces which have been properly roughened have shed new light on analytical applications of Raman spectroscopy [72]. Under the conditions of surface-enhanced Raman scattering (SERS), the absolute intensities of certain Raman bands are increased by a factor of 10^3 to

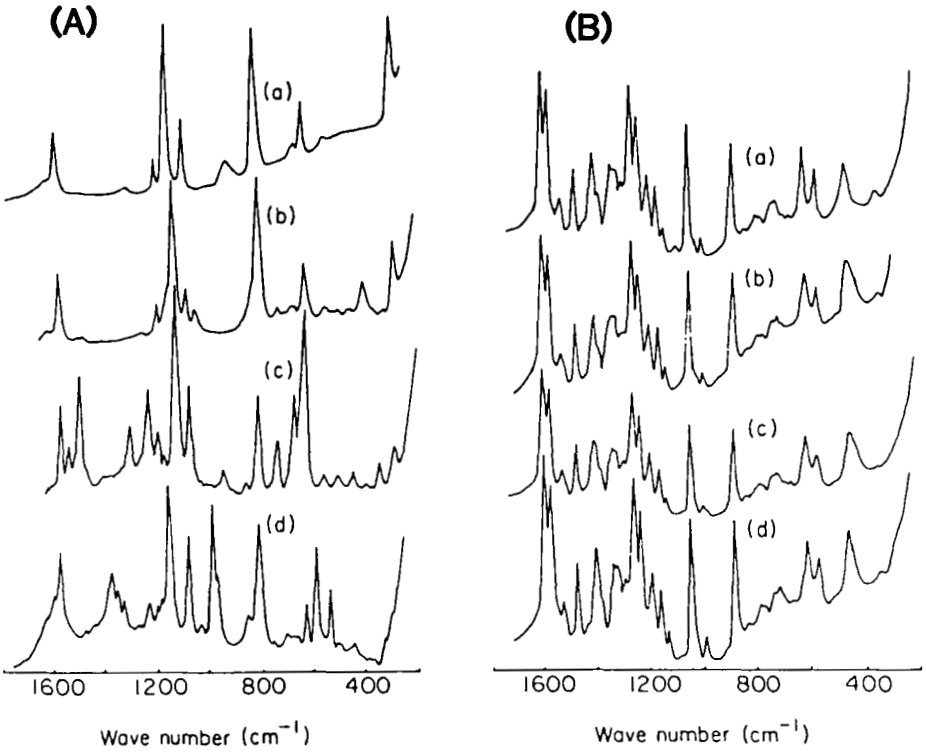

FIG. 15. (A) Raman spectra of some sulfonamides in about 0.1 M aqueous solutions: (a) sulfanilamide, (b) sulfaguanidine, (c) sulfathiazole, (d) sulfisomezole. (B) Resonance Raman spectra of the azo derivatives of some sulfonamides in 2×10^{-5} M aqueous solutions: (a) sulfanilamide, (b) sulfathiazole, (c) sulfapyridine, (d) sulfaguanidine. (Reprinted from Sato et al. [71] with permission. Copyright 1980, Elsevier Scientific Publishing Company.)

10^6 [72], and by use of the multiplicative effects of surface enhancement and resonance enhancement, detection limits lower than 10^{-9} M become possible [72]. The sensitivity of SERS is as good as that of luminescence techniques, with the additional advantage of the high selectivity inherent in vibrational spectroscopy. The SERS technique also offers a powerful means of obtaining high-quality Raman spectra from strongly fluorescent molecules. For analytical applications, SERS from silver colloidal systems are usually observed.

Torres and Winefordner [73] used SERS spectrometry for trace determination of nitrogen-containing drugs. Figures 16(a), 16(b), and

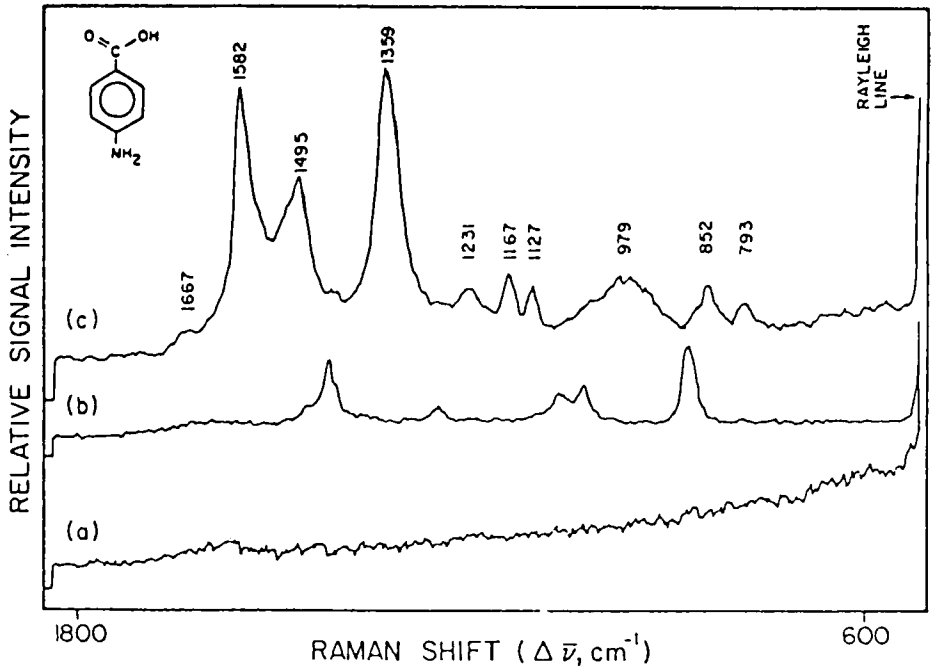

FIG. 16. (a) Raman spectrum of the silver hydrosols. (b) Raman spectrum of 80 μg/mL PABA in water. (c) SERS spectrum of 50 μg/mL PABA in silver hydrozols. (Reprinted from Torres and Winefordner [73] with permission. Copyright 1987, American Chemical Society.)

16(c), respectively, show the Raman spectrum of silver hydrosols, that of 80 μg/mL PABA (PABA; p-aminobenzoic acid) in water, and SERS spectrum of 50 μg/mL PABA in silver hydrosols [73]. Intense Raman features at 1582 and 1495 cm^{-1} in Fig. 16(c) are assignable to C−C stretching vibrations of the benzene ring of the PABA anion, and another strong peak at 1359 cm^{-1} in the same spectrum is attributed to a stretching vibration of its COO^- group. In contrast, all the bands observed in Fig. 16(b) are due to ethanol in the PABA solution. Therefore, a comparison of Fig. 16(c) with Fig. 16(b) clearly demonstrates high sensitivity of the SERS technique. Torres and Winefordner [73] found that the analytical calibration curve of PABA is linear over nearly 2 orders of magnitude, and that the detection limit is in the submicrogram-per-milliliter range. They also got a good calibration curve for 2-aminofluorene.

SERS spectrometry also seems promising for the direct identification of high-performance thin-layer chromatography (HPTLC) spots [72, 74-76]. In HPTLC/SERS analysis the dried HPTLC spots are spray wetted with silver colloidal solution, and the Raman spectra are measured directly from the spots by an ordinary 90° scattering arrangement. HPTLC spots down to subnanogram amounts of substances can be analyzed in situ by SERS/HPTLC spectrometry [72, 74-76]. This combined technique has been applied to trace determinations of dyes, nucleic acid building units, and some other organic compounds [72, 74-76].

D. Attempt at a Clinical Test by High-Performance Liquid Chromatography-Resonance Raman Combined Method

During the last decade the importance of high-performance liquid chromatography (HPLC) has increased remarkably for the analysis of biomedical materials [77]. In general, biological samples from a human body consist of many components and the amount of each component is very small. Accordingly, biomedical application of HPLC requires a suitable choice of column and detector. Iriyama et al. [78] proposed RR detection of physiological chromophores in the elute from HPLC.

RR detection has several unique advantages [78]. First, it is nondestructive, and therefore samples injected can be recovered in purified form. Second, use of the RR effect allows one to analyze chromophores selectively. Third, it is capable not only of chemical identification of a chromophore but also of its structure. Fourth, a commercial HPLC instrument can be combined with a Raman instrument without any interface.

The HPLC-RR system employed by Iriyama et al. [78] consists of HPLC, an UV detector, and a scanning-type Raman spectrometer equipped with a photomultiplier tube. The effluent from the column goes into a Raman cell via the UV detector. In Figs. 17(a) and 17(b) HPLC chromatograms and RR spectra of cytochrome c and met MbH_2O (Mb: myoglobin) are displayed, respectively [78]. The chromatograms were recorded at a wavelength of 280 nm by the UV detector, and the RR spectra were obtained by stopping the flow of the system at the retention times of cytochrome c and Mb. The sample volume injected was 20 μL for both cases (1.6 m$\underline{M}$). RR data provide knowledge about the types of hemes and their oxidation and spin states [78]. It is also possible to record chromatograms at a wavenumber of 1372 cm^{-1} by the Raman detector. The Raman detector set up at 1372 cm^{-1} is able to detect down to 20 μL of cytochrome c [78].

Iriyama et al. tried only artificial fluids of cytochrome c, met MbH_2O, and their mixture, and did not attempt body fluids [78]. However,

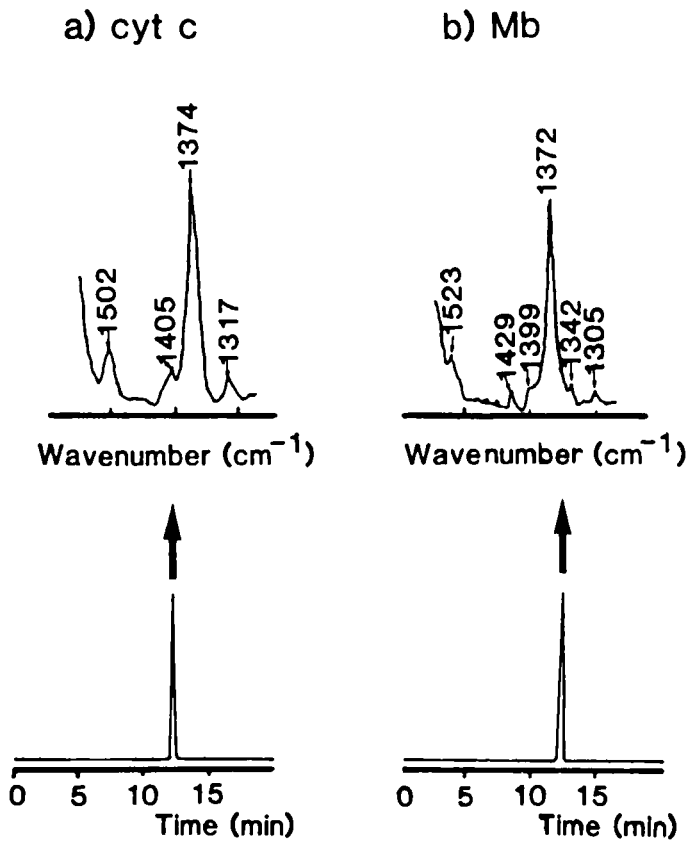

FIG. 17. Chromatograms monitored by an UV detector (280 nm) and corresponding RR spectra of cytochrome c (a) and met MbH_2O (b). (Reprinted from Iriyama et al. [78] with permission. Copyright 1983, Elsevier Scientific Publishing Co.)

a combined HPLC-RR system like the one described above may be useful for clinical tests of physiological chromophores such as porphyrins, carotenoides, and bilirubins in blood, urine, and so on. The use of a multichannel detector should permit measurement of the RR spectra of chromophores without stopping the system.

IV. PATHOLOGICAL EXAMINATION BY THE RAMAN MICROPROBE METHOD

The purpose of pathological examination is to diagnose a disease and elucidate its cause by investigating the morbidity of tissues and enucleated materials. Pathology optical and electron microscopes are routinely employed in the laboratory because morphological inquiry is primarily important for pathological examination. However, morphological observation is often not enough to know pathogenesis, and identification of a microscopic inclusion in the pathological specimens is occasionally required. Recent rapid progress in microbeam analytical techniques has provided pathologists with the opportunity of identifying the inclusion under optical or electron microscopes. The laser Raman microprobe, which is capable of nondestructive compound identification with a spatial resolution of 1 μm [10, 12-15], is a promising microanalytical technique for pathological examination. This microprobe consists of a laser light source, an optical microscope, and a Raman spectrometer. Besides nondestructive compound identification, the technique has the following advantages: (1) ease of sample preparation, (2) ability to provide information about molecular and crystal structures, and (3) the potential for simultaneous determination of chemical identification and distribution of an inclusion.

To the best of the author's knowledge, the first examples of microanalyses of pathological specimens in situ with the laser Raman microprobe method appeared in 1979. In that year Abraham and Etz [20] employed the micro-Raman technique to identify inclusions in an enlarged axillary lymph node from a patient with a silicone elastomer finger-joint prosthesis. In the same year Delhaye et al. [79] identified foreign material included in a histological section of fish liver as disordered graphite carbon by the use of the same technique, and Ballan-Dufrancais et al. [80] investigated purine concretions in various animal tissues. These pioneering works received attention from many pathologists as well as from Raman spectroscopists. The Raman microprobe is presently used extensively for the identification of inclusions in cancerous organs [22] and for the microanalysis of calculi [28] and gallstones [25, 26].

A. Identification of Inclusions in Lymph Node Tissue

Figure 18 shows a light micrograph of a stained section of the lymph node from a patient with a silicone elastomer finger-joint prosthesis [20]. This lymph node was changed to multinucleated giant cells by the invasion of foreign bodies; the arrowhead in Fig. 18 indicates one of

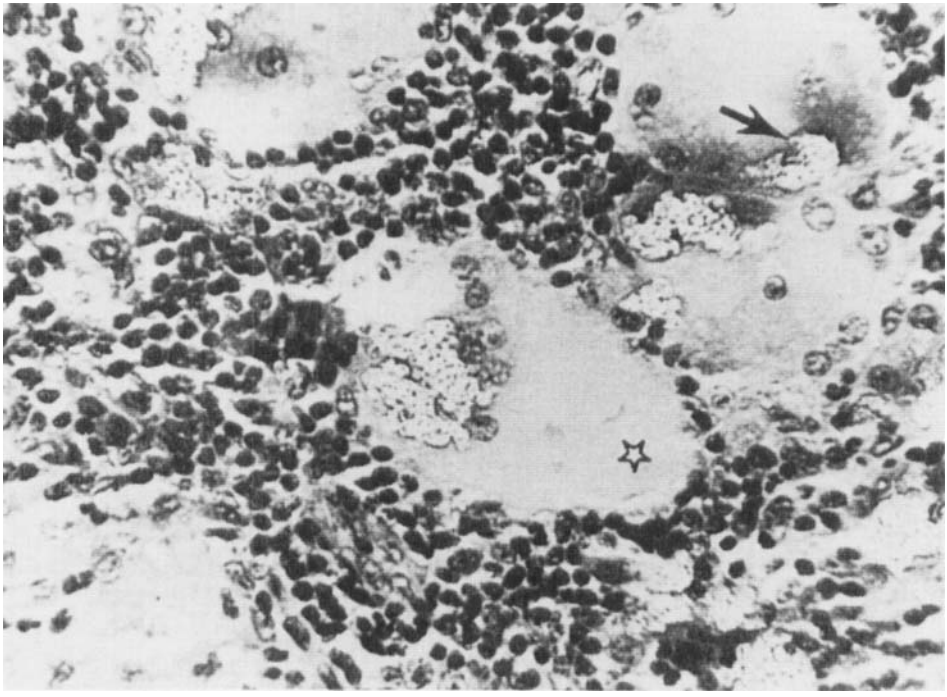

FIG. 18. Light micrograph of a stained section (5 μm) of lymph node with foreign bodies within multinucleated giant cells. This lymph node was obtained from an axilla of a patient with a silicone elastomer finger-joint prosthesis. Arrowhead indicates one of the foreign bodies and asterisk shows cytoplasmic area analyzed to take the Raman spectrum of the host tissue matrix. (Reprinted from Abraham and Etz [20] with permission. Copyright 1979, American Association for the Advancement of Science.)

the foreign bodies. Abraham and Etz [20] succeeded in identifying them in situ by the use of the Raman microprobe method. Raman spectra were measured for the inclusion (the arrowhead) and the cytoplasmic area (shown by an asterisk in Fig. 18) in the deparaffinized standard 5-μm section of the lymph node, mounted on a sapphire (α-Al_2O_3) substrate. The laser excitation line of 514.5 nm (40 mW at sample) was employed. The size of the inclusion was ~24 μm in diameter while the spot diameter of the laser beam was 16 μm [20]. For reference purposes the Raman spectrum was taken for a small (~60 μm) particle of silicone elastomer from a joint prosthesis with similar experimental

conditions. The spectrum obtained of the inclusion was clearly different from that of the cytoplasm and in good agreement with that of the silicone elastomer particle. Therefore, they concluded that the foreign bodies in the wrecked lymph node tissue were silicone rubber particles from the finger-joint prosthesis of the patient [20].

B. Identification of Inclusions in Lung Tissue

Buiteveld et al. [21] investigated inclusions in lung tissue from a silicosis patient by a Raman microprobe. Silicosis is caused by the accumulation of small airborne particles in lung tissue. Materials capable of making up the particles are silica, silicates, asbestos, or carbonates and related minerals. Identification of components of the particles is very important to clarify the source of the pollution which causes the disease.

Thin (5-15 μm) unstained sections of the lung tissue deposited on normal microscope slides were subjected to Raman measurements. The localization of the inclusions was performed with a polarized light microscopy. They varied in size between 2 and 4 μm in diameter, and the size of probe laser beam was 1.6 μm. The excitation wavelength employed was 514.5 nm, and the laser power at the samples was 4 mW.

Figure 19(a) shows the Raman spectrum of one of the inclusions [21]. The spectrum, characterized by an intense Raman band at 1085 cm^{-1} and weak to medium bands at 711, 281, and 155 cm^{-1}, was in very good agreement with a reference spectrum of calcite ($CaCO_3$) shown in Fig. 19(b). On the basis of this result, Buiteveld et al. [21] identified the inclusion as calcite. In this way most particles included in the lung tissue were found to be calcite, but some particles gave somewhat different spectra. They were very similar to that of magnesite ($MgCO_3$), revealing the existence of magnesite in the tissue.

Buiteveld et al. [21] compared the Raman measurements of unstained and stained specimens and the effect of laser power on the inclusions in the lung tissue and the tissue itself. According to them [21], the unstained specimens are much more suitable for Raman measurements because the stained specimens give a high background due to fluorescence of the staining dyes. With the unstained sections, however, the localization of small inclusions by polarized light microscopy is not always easy.

With regard to the effect of laser power, they found that the inclusions are more stable against high laser power than the tissue itself; a laser power density of 0.5×10^9 W/m^2 does not cause any damage to the inclusions whereas any density exceeding that value brings about visible damage to the tissue [21].

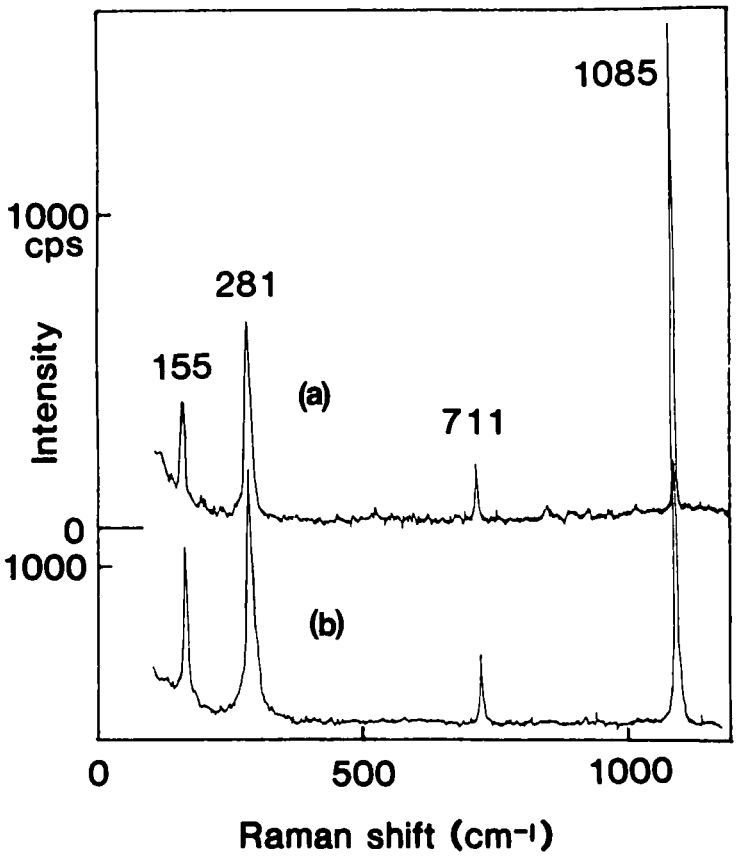

FIG. 19. (a) Raman spectrum of an inclusion in lung tissue from a patient with silicosis. (b) Raman spectrum of a reference calcite particle. (Reproduced from Buiteveld et al. [21] with permission. Copyright 1984, Society for Applied Spectroscopy.)

C. Investigation of Blue Particles in Cancerous Organs

The third example of pathological examinations by the Raman microprobe method is an investigation of blue particles in cancerous organs by Huong and Plouvier [22]. Blue particles are found in many samples obtained by direct apposition of cancerous tumors of human and animal origins. Figure 20(A) presents an example; a blue particle (arrow) in an unstained blood smear of a cancerous patient [22]. The particles have micrometer size without an apparent specific morphology and are

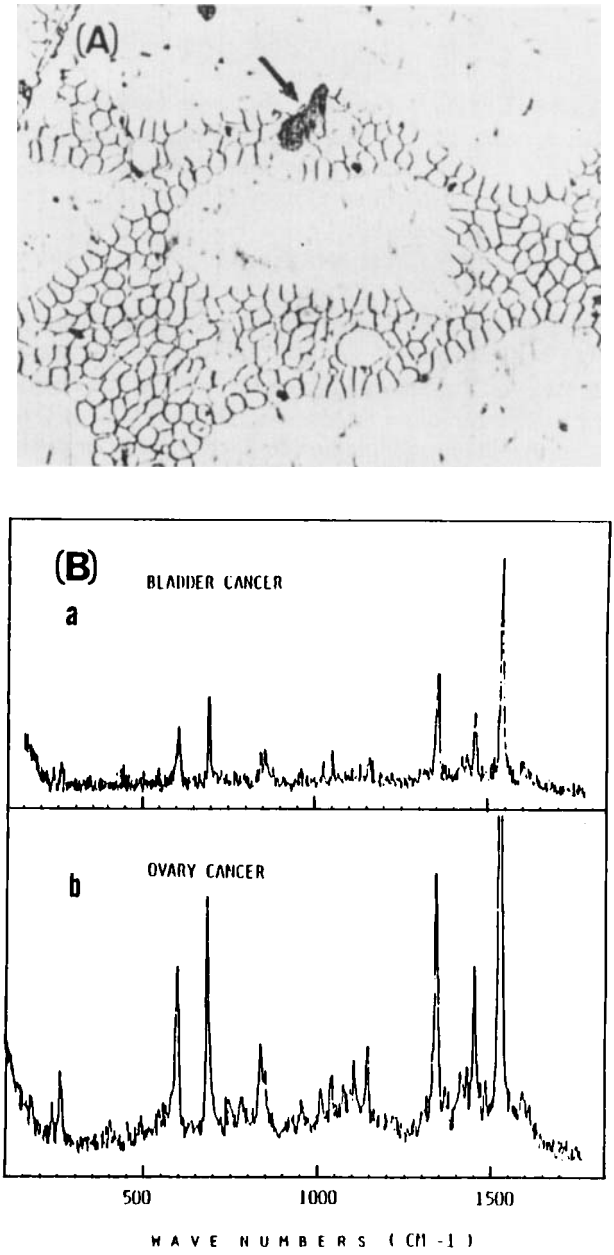

FIG. 20. (A) Blue particle (arrow) in unstained blood smear from a cancerous patient. (B) RR spectra of blue particles in cancerous organs: (a) bladder cancer, (b) ovary cancer. (Reprinted from Huong and Plouvier [22] with permission. Copyright 1984, Elsevier Science Publishers.)

considered to be of bacterial origin. Huong and Plouvier [22] measured the in situ RR spectra of the blue particles in several samples. Two examples of their RR spectra are presented in Fig. 20(B) [22]. The RR spectra of the blue particles are almost identical for samples of various cancerous and leukemic origins.

They also recognized, but less frequently, the presence of green particles in some samples where the blue particles were observed [22]. The RR spectra of the green particles are different from those of the blue ones, but again identical for samples of various origins.

Identification of the blue and green particles has not been achieved, but Huong and Plouvier have suggested, on the basis of the assignments of bands in the 300-240 cm^{-1} region to Cu-ligand stretching modes, that the colored particles correspond to two oxidation states of a copper-containing organometallic compound [22].

D. Microanalysis of Gallstones

Although it is known that cholelithiasis is caused by some metabolic abnormality, the detailed mechanism of gallstone formation is still unclear [81]. Microanalytical characterization of a gallstone is of particular importance because the gallstone microstructure reflects its formation history. Thus far, several kinds of physicochemical techniques, such as X-ray diffraction, gas and thin-layer chromatography, and IR spectroscopy, have been used for the microanalysis of gallstones. These techniques have individual advantages, but they are all destructive analytical methods. It is therefore impossible to examine a gallstone in situ. Ishida et al. [25, 26] and Zheng and Tu [27] recently introduced Raman spectroscopy to gallstone research. The former authors especially used Raman microprobe technique. The use of this technique allows the investigation of various components of a gallstone in a nondestructive manner under an optical microscope.

The stones investigated by Ishida et al. [25, 26] were a pure cholesterol gallstone, a pigment gallstone (bilirubin gallstone), a mixed stone consisting mainly of cholesterol and bilirubin, a calcium phosphate stone, and a fatty acid calcium-salt stone.

Microscopic observation of the pigment and the mixed stones demonstrated the presence of small white particles of 20-100 μm size in some spots. Traces (a) and (b) of Fig. 21 show the 514.5-nm excited Raman spectra of the white particles found in the mixed and pigment stones, respectively [25]. Figure 21 also includes Raman spectrum of zinc stearate (Trace c) for comparison purpose. The white particle spectra bear a general resemblance to that of zinc stearate; five major bands at 1470, 1445, 1300, 1130, and 1065 cm^{-1} arise from CH_2 bending,

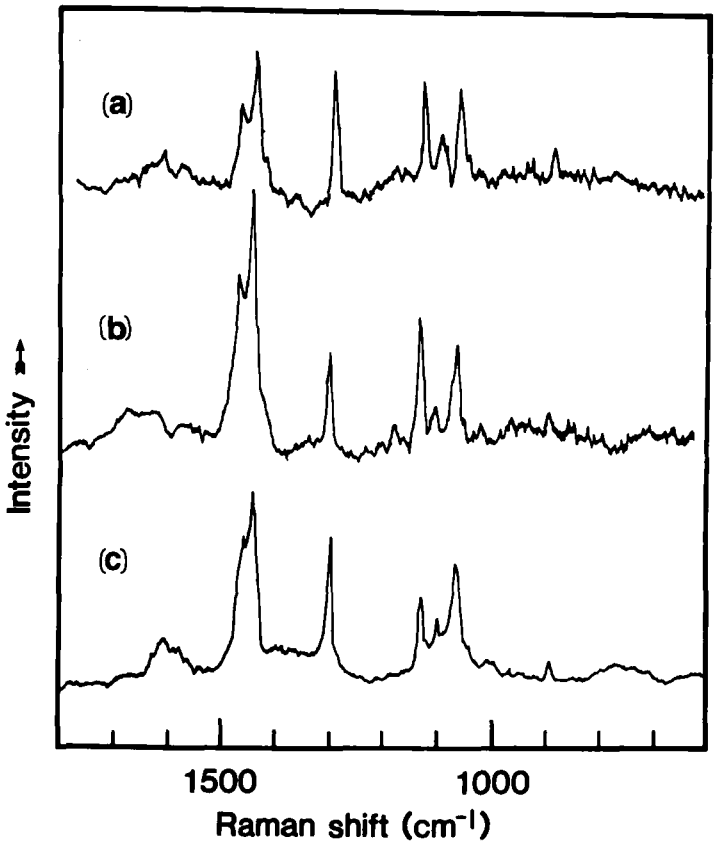

FIG. 21. (a), (b) Raman spectra of the white particles in the mixed (a) and pigment (b) stones. (c) Raman spectrum of zinc stearate. (Reproduced from Ishida et al. [25] with permission. Copyright 1987, Society for Applied Spectroscopy.)

CH_2 bending, CH_2 twisting, C−C skeletal stretching, and C−C skeletal stretching modes of a long methylene chain, respectively [25]. The 1445 cm^{-1} feature probably contains a band due to a symmetric stretching vibration of a carboxylate group. A weak band near 900 cm^{-1} is assigned to a $C-COO^-$ stretching mode. The results of the Raman microprobe experiment, together with those of FT-IR and EPMA (electron probe X-ray microanalysis), led Ishida et al. [25] to conclude that the white particles are composed mostly of the calcium salt of a fatty acid, probably crystalline calcium palmitate. Spectra similar to

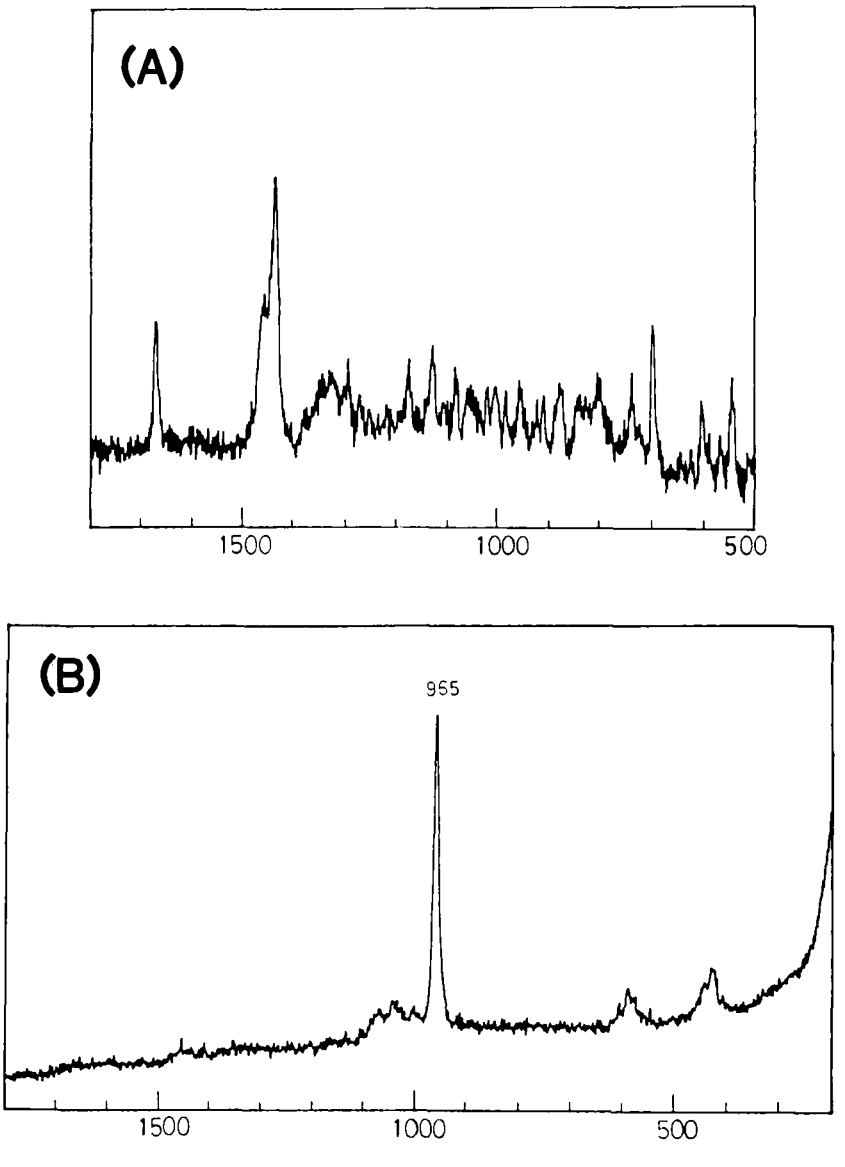

FIG. 22. (A) Raman spectrum of a transparent crystal in a fatty acid calcium-salt stone. (B) Raman spectrum of the outer layer of a calcium phosphate stone. (Reprinted from Ishida et al. [26] with permission. Copyright 1987, San Francisco Press.)

Traces (A) and (B) were obtained from several areas of the fatty acid calcium-salt stone.

The fatty acid calcium-salt stone contained a transparent crystal of 10 μm size in the white crystal of calcium palmitate. The identification of the transparent crystal was achieved by Raman microprobe measurement [26]. The spectrum obtained was almost identical to the reported spectrum of cholesterol as shown in Fig. 22(A), suggesting that the crystal is made of cholesterol [26].

The main ingredient of the calcium phosphate stone is calcium phosphate. Raman measurement is able to distinguish unambiguously two types of crystalline calcium phosphate, α- and β-$Ca_3(PO_4)_2$. The former is characterized by a single intense band at 968 cm^{-1} due to a PO symmetric stretching mode while the latter features an intense doublet at 971 and 948 cm^{-1} due to the same mode [82]. Figure 22(B) shows the Raman spectrum of the outer layer of the calcium phosphate stone. A similar spectrum was also obtained for the central part. Both spectra are almost identical with that of α-$Ca_3(PO_4)_2$, showing that the crystalline calcium phosphate included in the stone is of the α-type [26].

The studies of the five gallstones by Ishida et al. [25, 26] demonstrated that the unique advantages of the Raman microprobe method in gallstone research are its nondestructiveness and high spatial resolution. It was difficult for them to observe the distribution of gallstone components on a television monitor (Raman image) because of the strong background due to fluorescence. If "television monitoring" becomes possible by future progress in instrumentation, the usefulness of the Raman microprobe technique would become much greater.

V. CLINICAL DIAGNOSIS BY RAMAN SPECTROSCOPY

Recent rapid progress in medical engineering has produced new diagnostic tools. Some of them are based on spectroscopic techniques. The application of Raman spectroscopy in this area has not yet been realized, but it holds promise as a diagnostic tool for cataract formation [1, 29] and expiratory gas [32].

A. Cataract Diagnosis

Cataract is not a disease which causes a patient to die, but it comes to him as a great mental shock because he may become blind. Even advanced modern medicine can not restore a cataractous lens to normalcy, and therefore prevention of cataract formation is highly desirable. The remarkable development of laser-based spectroscopies gives rise to

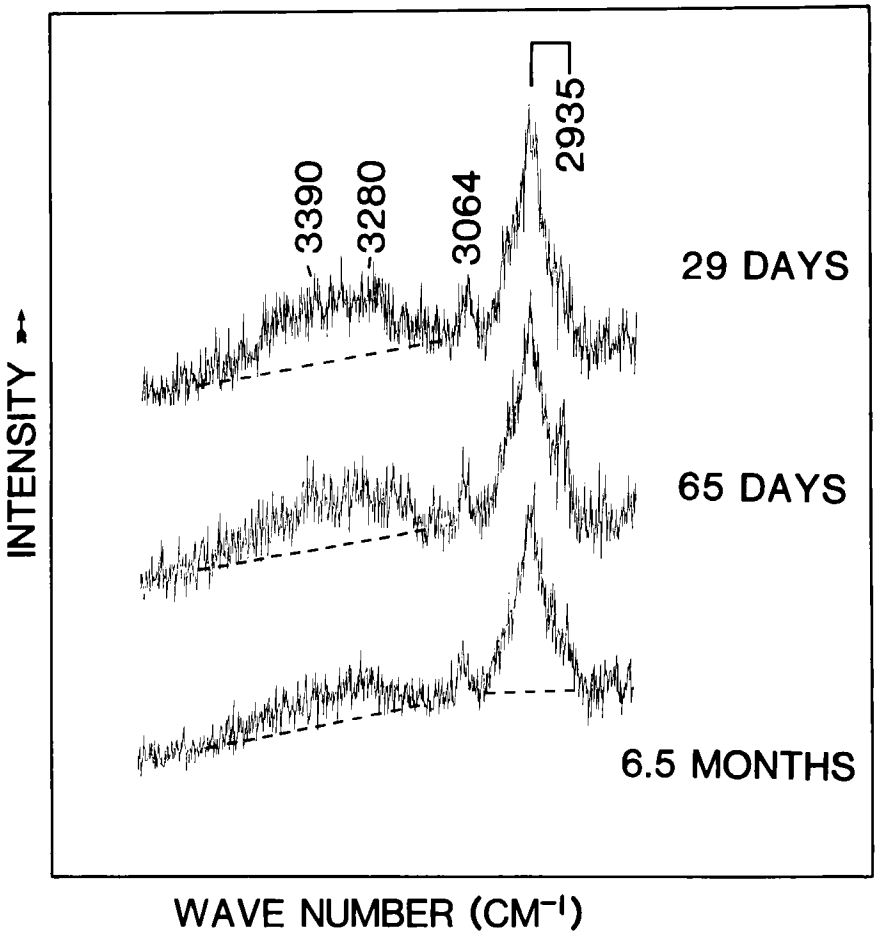

FIG. 23. Raman spectra in the 3800-2800 cm^{-1} region of SD-strain rat lens nuclei (29 and 65 days and 6.5 months old) measured by laser irradiation of 1 mW and 1 s (488.0 nm excitation). (Reprinted from Ozaki et al. [84] with permission. Copyright 1987, Society for Applied Spectroscopy.)

the expectation that senile cataracts can be foreseen at an ordinary medical examination.

Raman studies on lens aging and cataract formation, described in Section II-A, suggest the possibility of cataract diagnosis by Raman spectroscopy. For the clinical application of Raman spectroscopy, however, the following problems must be circumvented: (1) damage to the eye by laser light, (2) direct measurement of the Raman spectrum of the lens from a human eye, (3) strong fluorescence from a human eye lens, and (4) a diagnostic marker band for a precataractous lens. These problems have been under active investigation and are not far from complete solutions.

It is widely recognized that laser irradiation of 1 mW and 1 s (488.0-nm line of Ar laser) is below the threshold for retinal damage if the laser beam is out of focus for the retina. Therefore, for clinical applications it is crucial to show that one can measure the Raman spectrum of a lens with a laser irradiation of 1 mW and 1 s or less. Several years ago Mathies and Yu [83] succeeded in obtaining a Raman spectrum in the 1050-350 cm^{-1} region of an excised bovine lens with only 1 mW of laser power (514.5-nm line of Ar laser) using a SIT (SIT: silicon intensified target)-OMA (optical multichannel analyzer) system. However, it took them 11 min to do so. Their work was a great step forward, but it is still far from the goal. Ozaki et al. [84] recently exceeded the goal at a single stroke. Their Raman system consisted of a triple polychromator (Spex 1877), an intensified photodiode array detector (PAR 1422-1460), and a personal computer (NEC 9800). Figure 23 shows age-dependent Raman spectral changes in the 3800-2800 cm^{-1} region of an ICR strain mouse lens nuclei monitored by their system with a laser irradiation of only 1 mW and 1 s [84]. The signal-to-noise ratio of the spectra is not good, but it should be noted that the intensity decrease of the 3390 cm^{-1} band can be clearly observed. Their success strongly suggests that one can measure the Raman spectrum of a human lens without any damage to the eye.

In situ Raman measurements of intact lenses were reported independently by two groups in 1982. Mizuno et al. [85] obtained the Raman spectrum of the intact lens in a whole eyeball. An important conclusion from their work is that other portions of the eye, such as the cornea and the aqueous humor through which the laser beam passes, do not interfere with Raman signals from the lens. Yu et al. [42] went a step further; they reported the direct measurement of the Raman spectrum of the lens from a living rabbit. They put the rabbit under anesthesia because it took them a few minutes to take the Raman spectrum. It is presently possible to measure the Raman spectrum of a lens directly from a living animal without anesthesia; quite recently Bertoluzza et al.

TABLE 2

Raman Spectral Changes Observed for Lens Aging and Cataract Formation[a]

Raman bands	Lens aging[b]	Cataract formation		
		Emory mouse cataract[c]	Diabetic cataract[d]	Cac-strain mouse cataract[e]
OH stretching mode (3390 cm^{-1})	↓	↑	↑	↑
SH stretching mode (2579 cm^{-1})	↓	↓	↓	↓
S–S stretching mode (509 cm^{-1})	↑	↑	↑	↑[f]
Tyr doublet (I_{832}/I_{855})	↓	↑	↑	↑
Trp band (880 cm^{-1})	↓	↓	↓	↓

[a](↑) intensity increase; (↓) intensity decrease.
[b]Ref. 43.
[c]Ref. 51.
[d]Refs. 47 and 48.
[e]Ref. 49.
[f]Not clear because of the rising background.

[86] succeeded in obtaining the Raman spectrum of an intact lens directly from a living rabbit with a laser irradiation of 2 mW and 0.5 s. In this way, Problems (1) and (2) are nearly solved.

In contrast to Problems (1) and (2), Problem (3) is still unsolved because some aged human lenses emit strong fluorescence even with 647.1-nm excitation [87]. A human lens exhibits several fluorophors such as blue fluorophor (maximum at 440 nm with an UV excitation at 345 nm), blue-green fluorophor (maximum at 495 nm with an excitation at 406.7 nm), and red fluorophor (maximum at 670 nm with an excitation at 647.1 nm) [87, 88]. The intensities of these fluorophores are very weak or nearly zero for young human lenses, but they increase gradually with aging and the fluorescence maximum of a human lens moves to a longer wavelength. Therefore, longer wavelength excitation must be employed with age to obtain the Raman spectrum of a human lens [87, 88]. According to Yu et al. [87], most human lenses of persons above age 60 give reasonable spectra with 647.1-nm excitation, but it appears to be difficult to find an excitation wavelength which provides passable spectra for all human lenses, unless one uses near-infrared excitation. A practical solution for the fluorescence problem may be to employ the 647.1-nm excitation in every case, and when a lens emits strong fluorescence (red fluorophor) which interferes with the Raman spectrum, it should be recognized as pathological or prepathological because the appearance of red fluorophor may be a sign of a cataract [87].

Another important step in the development of Raman spectroscopy for cataract diagnosis is to determine a diagnostic marker band for precataractous signatures. The marker band must be specific for cataract formation, and thus it can be picked out from a comparison of the Raman spectral changes for cataract formation with those for normal lens aging. Table 2 summarizes the spectral changes observed for cataract formation and normal lens aging. Bands which show different behaviors for cataract formation and lens aging are the OH stretching band at 3390 cm^{-1} and the tyrosine doublet near 840 cm^{-1}. Of these, the OH stretching band seems to be more promising because of the following reasons. First, the intensity of the OH stretching band is very strong and its change with cataract formation can be clearly detected [50, 51]. Second, the change is observable even in a precataractous stage [51]. Third, the band is located in the highest frequency region of the lens spectrum, and therefore suffers the least from fluorescence interference. However, it must be kept in mind that Table 2 is concerned with mouse and rat lenses. Accordingly, it is now very important to determine whether the OH stretching band is useful for human senile cataracts or not.

Yu et al. [88] proposed that the intensity ratio of a fluorescence band and a Raman peak (F/R) be used as a diagnostic marker for precataractous symptoms. They think that the intensity of lens fluorescence is more sensitive to various pathological disturbances in a lens than that of a Raman band.

B. Analysis of Expiration

Analysis of the expired air of a patient under an anesthetic is very important for controlling anesthesia. Expiration analysis is also useful for the diagnosis of pulmonary diseases such as silicosis and pulmonary asbestosis. However, real time monitoring of human expiration has not always been easy. Albrecht et al. [32] proposed in situ analysis of human expiratory gas by Raman spectroscopy. When Raman spectroscopy is employed for the analysis of a mixed gas like the expiratory gas, two major problems must be overcome. One is the method which enhances

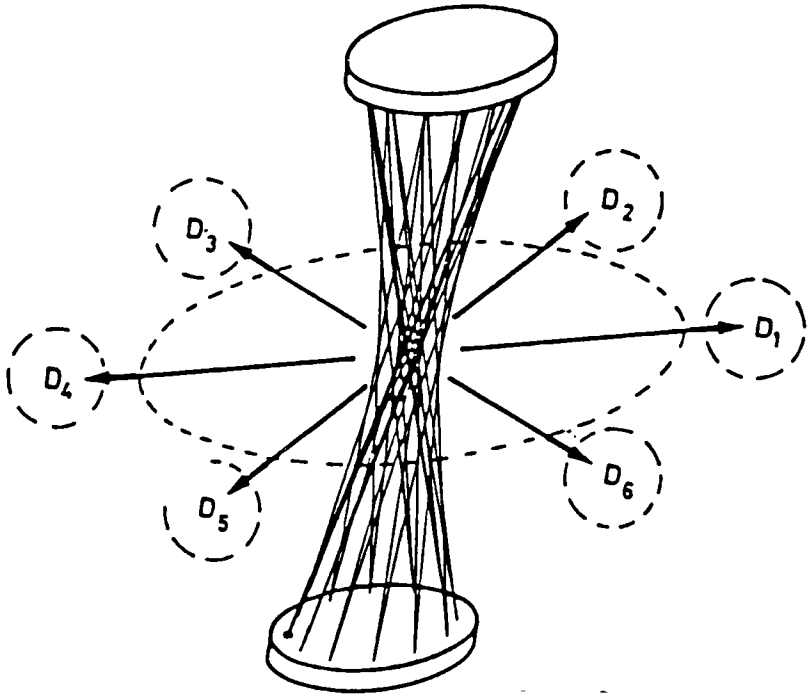

FIG. 24. A multipass cell and six detectors for the analysis of human expiration. (Reproduced from Albrecht et al. [32] with permission. Copyright 1977, Fachverlag Schiele & Schon.)

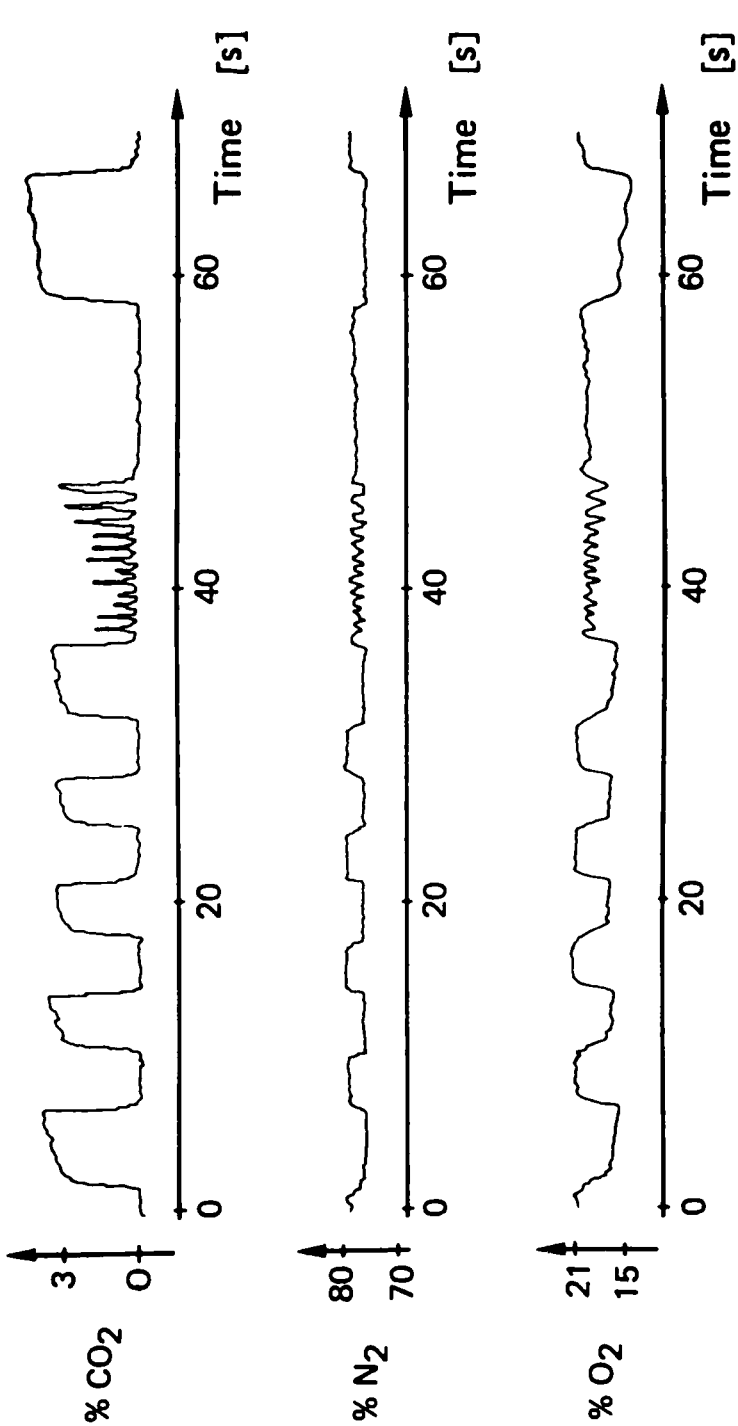

FIG. 25. Time-dependent changes of CO_2, N_2, and O_2 concentrations of human expired air monitored by Raman spectroscopy. (Reprinted from Albrecht et al. [32] with permission. Copyright 1977, Fachverlag Schiele & Schon.)

the intensities of observed Raman bands. Another is the method which estimates the relative concentration of each component of the expired air. In order to solve the first problem, Albrecht et al. [32] used the multipass cell shown in Fig. 24. Inside the cell the unpolarized laser beam is reflected back and forth up to 70 times, and the power density there is about the same as inside the laser resonator. The second problem was settled by arranging six detectors (photomultiplier tube) around the cell in a plane perpendicular to the cell axis. An interference filter was placed in front of each detector, and in this way each detector was able to detect a specific Raman line selectively. This device enabled them to observe six different components of the expiratory gas simultaneously.

Figure 25 shows time-dependent changes of CO_2, N_2, and O_2 concentrations in the expiratory gas of a human patient [32]. From the results in Fig. 25 the respiratory interval as well as relative concentrations of CO_2, N_2, and O_2 gases can be determined. Their proposal was made about 10 years ago [32], so it is now probably possible for six detectors to be replaced by one multichannel detector.

VI. FUTURE PROSPECTS

The wide variety of topics described above can be divided into basic research on biomedical materials and clinical applications. These two areas must continue to make parallel progress. With regard to the first, in situ Raman measurements of cells, tissues, and organs must be carried out more frequently. Such attempts will provide new insight into the structure and function of constituents of biological materials because unique information about them can be obtained under conditions where the materials maintain their normal functions.

In order to measure the Raman spectra of the cells, tissues, and organs satisfactorily, however, two major problems must be circumvented. These are fluorescence from samples and/or impurities which intrinsically mask weaker Raman scattering and damage to samples by strong laser illumination. Biological materials, especially morbid ones, often emit strong fluorescence. Therefore, the solution to the fluorescence problem is the key to making great strides in the Raman study of biomedical materials. The best solution to elimination of the fluorescence of biomedical materials is probably to change the excitation wavelength further into the red. In this respect the development of detectors with high-sensitivity in the red and progress in near-infrared Raman spectroscopy [89] and Fourier-transform Raman spectroscopy [90, 91] are very much to be desired. Optical depletion of luminescent impurities

by pulsed-laser excitation may also be useful to get around the fluorescence [92].

Excitation in the longer wavelength region is also very effectual for avoiding sample decomposition. The use of a multichannel detector with high sensitivity is, of course, very much preferable for photolabile samples since it greatly reduces the measurement time.

As for the clinical applications, it seems very likely that some of them will be put to practical use in the near future. In my opinion, cataract diagnosis, blood testing, and expiration analysis by Raman spectroscopy hold considerable potential for practical use. Real-time analysis is inevitable for clinical applications, and thus progress in multichannel spectroscopy, including the development of new detectors, signal processing, and computer software, is needed. Automatization of Raman measurement must also be investigated.

As a future target of clinical application of Raman spectroscopy, Raman measurement under an endoscope seems to be very interesting. Laser-based electronic absorption and fluorescence spectroscopy using an endoscope has already been used for the diagnosis of internal organs. In like manner, an endoscopic examination using Raman spectroscopy also may play a unique role in clinical diagnosis because vibrational spectroscopy is intrinsically information-rich.

Acknowledgments

I thank Professor M. Tsuboi for giving me a chance to write this review article, and Dr. E. S. Etz and Professors J. C. Banford, A. Bertoluzza, K. Iriyama, T. Kitagawa, G. J. Thomas Jr., and A. T. Tu for providing me with preprints and reprints.

REFERENCES

[1] Y. Ozaki and K. Iriyama, "Potential of Raman Spectroscopy in Medical Science," in Laser Scattering Spectroscopy of Biological Objects (J. Stepanek, P. Anzenbacher, and B. Sedlacek, eds.), Elsevier, Amsterdam, 1987.

[2] P. R. Carey, Biochemical Applications of Raman and Resonance Raman Spectroscopies, Academic, New York, 1982.

[3] A. T. Tu, Raman Spectroscopy in Biology, Wiley, New York, 1982.

[4] F. S. Parker, Applications of Infrared, Raman, and Resonance Raman Spectroscopy in Biochemistry, Plenum, New York, 1983.

[5] R. J. H. Clark and R. E. Hester (eds.), Advances in Spectroscopy, Vol. 13, Wiley-Heyden, London, 1986.
[6] T. G. Spiro (ed.), Biological Applications of Raman Spectroscopy, Wiley, New York, 1987.
[7] K. A. Hartman, N. W. Clayton, and G. J. Thomas Jr., Biochem. Biophys. Res. Commun., 50, 942 (1973).
[8] N.-T. Yu, B. H. Jo, R. C. C. Chang, and J. D. Huber, Arch. Biochem. Biophys., 160, 614 (1974).
[9] K. Larsson and L. Hellgren, Experientia, 30, 481 (1974).
[10] M. Bridoux and M. Delhaye, "Time-Resolved and Space-Resolved Raman Spectroscopy," in Advances in Infrared and Raman Spectroscopy, Vol. 2 (R. J. H. Clark and R. E. Hester, eds.), Wiley-Heyden, London, 1976.
[11] H. Hamaguchi, Appl. Spectrosc. Rev., 24, 137 (1988).
[12] M. Delhaye and P. Dhamelincourt, J. Raman Spectrosc., 3, 33 (1975).
[13] G. J. Rosasco, E. S. Etz, and W. A. Cassatt, Appl. Spectrosc., 29, 396 (1975).
[14] P. Dhamelincourt, F. Wallart, M. Leclercq, A. T. N'Guyen, and D. O. Landon, Anal. Chem., 51, 414A (1979).
[15] G. J. Rosasco, "Raman Microprobe Spectroscopy," in Advances in Infrared and Raman Spectroscopy, Vol. 7 (R. J. H. Clark and R. E. Hester, eds.), Wiley-Heyden, London, 1980.
[16] G. J. Thomas Jr., "Applications of Raman Spectroscopy in Structural Studies of Viruses, Nucleoproteins, and Their Constituents," in Ref. 5.
[17] G. J. Thomas Jr., "Viruses and Nucleoproteins," in Ref. 6, Vol. 1.
[18] S. J. Webb and R. Lee, IRCS Med. Sci., 5, 102 (1977).
[19] J. C. Banford, D. H. Brown, A. A. McConnell, C. J. McNeil, W. E. Smith, R. A. Hazelton, and R. D. Sturrock, Analyst, 107, 195 (1982).
[20] J. L. Abraham and E. S. Etz, Science, 206, 716 (1979).
[21] H. Buiteveld, F. F. M. De Mul, J. Mud, and J. Greve, Appl. Spectrosc., 38, 304 (1984).
[22] P. V. Huong and S. R. Plouvier, J. Mol. Struct., 115, 489 (1984).
[23] F. F. M. De Mul, H. Buiteveld, J. Lankester, J. Mud, and J. Greve, Human Pathol., 15, 1062 (1984).
[24] E. S. Etz, B. B. Tomazic, and W. E. Brown, Microbeam Anal., p. 39 (1986).
[25] H. Ishida, R. Kamoto, S. Uchida, A. Ishitani, Y. Ozaki, K. Iriyama, E. Tsukie, K. Shibata, F. Ishihara, and H. Kameda, Appl. Spectrosc., 41, 407 (1987).

[26] H. Ishida, Y. Ozaki, K. Kamoto, A. Ishitani, K. Iriyama, I. Takagi, E. Tsukie, K. Shibata, F. Ishihara, and H. Kameda, Microbeam Anal., p. 189 (1987).
[27] (a) S. Zheng and A. T. Tu, Appl. Spectrosc., 40, 1099 (1986). (b) S. Zheng and A. T. Tu, Ibid., 41, 696 (1987).
[28] M. Daudon, M. F. Protat, R. J. Reveillaud, and H. Jaeschke-Boyer, Kidney Int., 23, 842 (1983).
[29] Y. Ozaki, A. Mizuno, K. Itoh, and K. Iriyama, Innov. Tech. Biol. Med., 5, 269 (1984).
[30] N.-T. Yu, D. C. DeNagell, D. J.-Y. Ho, and J. F. R. Kuck, "Ocular Lenses," in Ref. 6, Vol. 1.
[31] Y. Ozaki, A. Mizuno, K. Itoh, and K. Iriyama, "Structure and Function of the Lens Proteins Studied by Raman Spectroscopy," in Spectroscopic and Structural Studies of Biomedical Materials (J. Twardowski, ed.), Sigma Press, London, 1988.
[32] H. Albrecht, G. Muller, and M. Schaldach, Biomed. Technol., 22, 361 (1977).
[33] D. C. O'Shea, M. L. Bartlett, and R. A. Young, Arch. Oral Biol., 19, 995 (1974).
[34] M. Yamada, H. Horibe, K. Fujimori, S. Yamashita, and T. Yamashita, Cell. Molec. Biol., 25, 167 (1979).
[35] K. Nishigori, M. Yamada, K. Fujimori, K. Chikamori, and S. Yamashita, Acta Histochem. Cytochem., p. 599 (1979).
[36] M. Nishino, S. Yamashita, T. Aoba, M. Okazaki, and Y. Moriwaki, J. Dent. Res., 60, 751 (1981).
[37] M. Suzuki, H. Kato, S. Wakumoto, G. Katagiri, and A. Ishitani, J. Raman Spectrosc., 18, 315 (1987).
[38] E. Cotlier, "The Lens," in Adler's Physiology of the Eye (R. A. Moses, ed.), Mosby, St. Louis, 1981.
[39] H. Bloemendal (ed.), Molecular and Cellular Biology of the Eye Lens, Wiley, New York, 1981.
[40] R. A. Schachar and S. A. Solin, Invest. Ophthalmol., 14, 380 (1975).
[41] N.-T. Yu and E. J. East, J. Biol. Chem., 250, 2196 (1975).
[42] N.-T. Yu, J. F. R. Kuck Jr., and C. C. Askren, Curr. Eye Res., 1, 615 (1982).
[43] Y. Ozaki, A. Mizuno, K. Itoh, and K. Iriyama, J. Biol. Chem., 262, 15545 (1987).
[44] Y. Ozaki, A. Mizuno, K. Itoh, M. Yoshiura, T. Iwamoto, and K. Iriyama, Biochemistry, 22, 6254 (1983).
[45] Y. Ozaki and K. Iriyama, Technical Digest of IQEC '88, Tokyo, 1988, p. 453.

[46] M. N. Siamwiza, R. C. Lord, M. C. Chen, T. Takamatsu, I. Harada, H. Matsuura, and T. Shimanouchi, Biochemistry, 14, 4870 (1975).
[47] Y. Ozaki, A. Mizuno, Y. Kamada, K. Itoh, and K. Iriyama, Chem. Lett., p. 887 (1982).
[48] A. Mizuno, H. Nozawa, T. Yaginuma, H. Matsuzaki, Y. Ozaki, and K. Iriyama, Exp. Eye Res., 45, 185 (1987).
[49] K. Itoh, Y. Ozaki, A. Mizuno, and K. Iriyama, Biochemistry, 22, 1773 (1983).
[50] K. Iriyama, A. Mizuno, Y. Ozaki, K. Itoh, and H. Matsuzaki, Curr. Eye Res., 2, 489 (1983).
[51] Y. Ozaki, A. Mizuno, K. Itoh, S. Matsushima, and K. Iriyama, Appl. Spectrosc., 41, 597 (1987).
[52] D. M. Thomas and K. L. Schepler, Invest. Ophthalmol. Vis. Sci., 19, 904 (1980).
[53] A. Mizuno, Y. Ozaki, K. Itoh, S. Matsushima, and K. Iriyama, Biochem. Biophys. Res. Commun., 119, 989 (1984).
[54] Y. Tonomura, Muscle Proteins, Muscle Contraction and Cation Transport, University of Tokyo Press, Tokyo, 1973.
[55] I. M. Asher, E. B. Carew, and H. E. Stanley, "Laser Raman Spectroscopy; A New Probe of the Molecular Conformations of Intact Muscle and Its Components," in Physiology of Smooth Muscle (E. Bulbring and M. F. Shuba, eds.), Raven Press, New York, 1976.
[56] M. Pezolet, M. Pigeon-Gosselin, and J.-P. Caille, Biochim. Biophys. Acta, 533, 263 (1978).
[57] M. Pezolet, M. Pigeon-Gosselin, J. Nadeau, and J.-P. Caille, Biophys. J., 31, 1 (1980).
[58] J.-P. Caille, M. Pigeon-Gosselin, and M. Pezolet, Biochim. Biophys. Acta, 758, 121 (1983).
[59] J. A. Jurnak and A. McPherson (eds.), Biological Macromolecules and Assemblies, Vol. 1: Virus Structures, Wiley, New York, 1984.
[60] G. J. Thomas Jr. and L. A. Day, Proc. Natl. Acad. Sci. U.S.A., 78, 2962 (1981).
[61] G. J. Thomas Jr., B. Prescott, and L. A. Day, J. Mol. Biol., 165, 321 (1983).
[62] J. Finer-Moore, R. M. Stroud, B. Prescott, and G. J. Thomas Jr., J. Biomolec. Struct. Dynam., 2, 93 (1984).
[63] G. J. Thomas Jr., Spectrochim. Acta, 41, 217 (1985).
[64] F. Adar and M. Erecinska, Biochemistry, 17, 5484 (1978).
[65] R. A. Young, J. Dent. Res., 53B, 193 (1974).

[66] F. Brudevold and R. Soremark, "Chemistry of the Mineral Phase of Enamel," in Structural and Chemical Organization of Teeth, Vol. II (A. E. W. Miles, ed.), Academic, New York, 1967.
[67] M. Friedman, The Chemistry and Biochemistry of the Sulfhydryl Group in Amino Acids, Peptides and Proteins, Pergamon, Oxford, 1973.
[68] M. D. Morris, Anal. Chem., 47, 2453 (1975).
[69] M. S. Rahaman and M. D. Morris, Talanta, 23, 65 (1976).
[70] M. D. Morris, Anal. Lett., 9, 469 (1976).
[71] S. Sato, S. Higuchi, and S. Tanaka, Anal. Chim. Acta, 120, 209 (1980).
[72] E. Koglin and J.-M. Sequaris, "Surface Enhanced Raman Scattering of Biomolecules," in Topics in Current Chemistry, Vol. 134, Springer-Verlag, Berlin, 1986.
[73] E. L. Torres and J. D. Winefordner, Anal. Chem., 59, 1626 (1987).
[74] (a) C. D. Tran, J. Chromatogr., 292, 432 (1984). (b) C. D. Tran, Anal. Chem., 56, 824 (1984).
[75] J.-M. L. Sequaris and E. Koglin, Anal. Chem., 59, 525 (1987).
[76] E. Koglin, Abstract Book of 39th Pittsburgh Conference, p. 924 (1988).
[77] Chromatographic Science Series, Vol. 1-, Dekker, New York.
[78] K. Iriyama, Y. Ozaki, H. Hibi, and T. Ikeda, J. Chromatogr., 254, 285 (1983).
[79] M. Delhaye, P. Dhamelincourt, and F. Wallart, Toxicol. Environ. Chem. Res., 3, 73 (1979).
[80] C. Ballan-Dufrancais, M. Truchet, and P. Dhamelincourt, Biol. Cellulaire, 36, 51 (1979).
[81] J. M. Kissane (ed.), Anderson's Pathology, Mosby, St. Louis,
[82] A. Bertoluzza, M. A. Battaglia, R. Simoni, and D. A. Long, J. Raman Spectrosc., 14, 178 (1983).
[83] R. Mathies and N.-T. Yu, Ibid., 7, 349 (1978).
[84] Y. Ozaki, K. Iriyama, and H. Hamaguchi, Appl. Spectrosc., 41, 1245 (1987).
[85] A. Mizuno, Y. Ozaki, Y. Kamada, H. Miyazaki, K. Itoh, and K. Iriyama, Curr. Eye Res., 1, 609 (1982).
[86] A. Bertoluzza, C. Fagnano, P. Monti, R. Caramazza, E. Barbaresi, and S. Mancini, Proceedings of 2nd European Conference on the Spectroscopy of Biological Molecules, Freiburg, 1987.
[87] N.-T. Yu, J. F. R. Kuck Jr., and C. C. Askren, Invest. Ophthalmol. Vis. Sci., 18, 1278 (1979).

[88] N.-T. Yu, M. Bando, and J. F. R. Kuck Jr., Ibid., 26, 97 (1985).
[89] M. Fujiwara, H. Hamaguchi, and M. Tasumi, Appl. Spectrosc., 40, 137 (1986).
[90] T. Hirschfield and B. Chase, Ibid., 40, 133 (1986).
[91] D. J. Moffatt, H. Buijs, and W. F. Murphy, Ibid., 40, 1079 (1986).
[92] H. Hamaguchi, T. Tahara, and M. Tasumi, Ibid., 41, 1265 (1987).